

Multi-Tubal Rank of Third Order Tensor and Related Low Rank Tensor Completion Problem

Quan Yu*, Xinzhen Zhang[†] and Zheng-Hai Huang[‡]

December 10, 2020

Abstract. Recently, a tensor factorization based method for a low tubal rank tensor completion problem of a third order tensor was proposed, which performed better than some existing methods. Tubal rank is only defined on one mode of third order tensor without low rank structure in the other two modes. That is, low rank structures on the other two modes are missing. Motivated by this, we first introduce multi-tubal rank, and then establish a relationship between multi-tubal rank and Tucker rank. Based on the multi-tubal rank, we propose a novel low rank tensor completion model. For this model, a tensor factorization based method is applied and the corresponding convergence analysis is established. In addition, spatio-temporal characteristics are intrinsic features in video and internet traffic tensor data. To get better performance, we make full use of such features and improve the established tensor completion model. Then we apply tensor factorization based method for the improved model. Finally, numerical results are reported on the completion of image, video and internet traffic data to show the efficiency of our proposed methods. From the reported numerical results, we can assert that our methods outperform the existing methods.

Key words. Tensor factorization, tensor completion, tubal rank, spatio-temporal characteristics.

AMS subject classifications. 15A69,46B28

1 Introduction

A tensor is a multidimensional array, and an N th-order tensor is an element of the tensor product space of N vectors, which have their own dimensions [17]. Tensors, as higher order generalizations of vectors and matrices, have wide applications in various fields [4, 7, 8, 13, 19, 20, 22, 26, 30, 36]. Tensor decompositions, various generalizations of matrix singular value decomposition, have attracted more and more attentions, including CANDECOMP/PARAFAC (CP) decomposition [6, 14], Tucker decomposition [34] and tensor singular value decomposition (SVD) [9, 11, 15, 16, 28]. Corresponding to such tensor decompositions,

*School of Mathematics, Tianjin University, Tianjin 300354, P.R. China. E-mail: QuanYu527@163.com.

[†]School of Mathematics, Tianjin University, Tianjin 300354, P.R. China. E-mail: xzzhang@tju.edu.cn. Her work is supported by NSFC (11871369).

[‡]School of Mathematics, Tianjin University, Tianjin 300354, P.R. China. E-mail: huangzhenghai@tju.edu.cn. His work is supported by NSFC (11871051).

tensor ranks are called the CP rank, Tucker rank and tubal rank, respectively.

Third order tensors are widely used in chemometrics [29, 32], psychometrics [18] and image inpainting [5, 23, 25, 42]. Unless otherwise specialized, tensors in this paper are of third order. For a third order (n_1, n_2, n_3) -dimensional tensor $\mathcal{X} \in \mathbb{R}^{n_1 \times n_2 \times n_3}$, the CP decomposition is to decompose \mathcal{X} as a sum of some outer products of three vectors:

$$\mathcal{X} = \sum_{i=1}^r a_1^{(i)} \circ a_2^{(i)} \circ a_3^{(i)},$$

where the symbol “ \circ ” denotes the outer product and $a_j^{(i)} \in \mathbb{R}^{n_j}$ is a vector ($i \in \{1, 2, \dots, r\}$ and $j \in \{1, 2, 3\}$). The smallest r in CP decomposition is called CP rank of \mathcal{X} . From [10], it is NP-hard to determine the CP rank. Compared with CP rank, Tucker rank is easy to compute, and hence most of low rank tensor completion and recovery models are based on Tucker rank. Precisely, Tucker rank is a vector of the matrix ranks

$$\text{rank}_{TC}(\mathcal{C}) = (\text{rank}(C_{(1)}), \text{rank}(C_{(2)}), \text{rank}(C_{(3)})),$$

where $C_{(1)} \in \mathbb{R}^{n_1 \times (n_2 n_3)}$ ($C_{(2)} \in \mathbb{R}^{n_2 \times (n_1 n_3)}$ and $C_{(3)} \in \mathbb{R}^{n_3 \times (n_1 n_2)}$) is mode-1 (mode-2 and mode-3, respectively) matricization of tensor. More recently, Kilmer *et al.* [15] introduced tensor-tensor product (t-product) and tensor singular value decomposition (t-SVD). Based on these definitions, tubal rank was introduced and studied in [15, 16, 28].

The low rank tensor completion problem is to find a low rank tensor from observed incomplete data, which arises from various fields including internet traffic recovery [1, 2, 33, 41], image and video inpainting [12, 21, 22, 42]. Low rank tensor completion is modeled as

$$\min_{\mathcal{C}} \text{rank}(\mathcal{C}), \quad \text{s.t.} \quad P_{\Omega}(\mathcal{C}) = P_{\Omega}(\mathcal{M}), \quad (1)$$

where $\text{rank}(\cdot)$ is a tensor rank and Ω is an index set locating the observed data. P_{Ω} is a linear operator that extracts the entries in Ω and fills the entries not in Ω with zeros, and \mathcal{M} is a given tensor.

Different tensor ranks lead to different low rank tensor completion models of (1) with different methods. The following low Tucker rank tensor completion is considered

$$\min_{\mathcal{C}} (\text{rank}(C_{(1)}), \text{rank}(C_{(2)}), \text{rank}(C_{(3)})), \quad \text{s.t.} \quad P_{\Omega}(\mathcal{C}) = P_{\Omega}(\mathcal{M}).$$

To keep things simple, the weighted Tucker rank minimization problems is formulated as

$$\min_{\mathcal{C}} \sum_{i=1}^3 \text{rank}(C_{(i)}), \quad \text{s.t.} \quad P_{\Omega}(\mathcal{C}) = P_{\Omega}(\mathcal{M}). \quad (2)$$

Note that problem (2) is non-convex since matrix rank function is nonconvex. To solve (2), the convex optimization problem is considered as

$$\min_{\mathcal{C}} \sum_{i=1}^3 \|C_{(i)}\|_*, \quad \text{s.t.} \quad P_{\Omega}(\mathcal{C}) = P_{\Omega}(\mathcal{M}). \quad (3)$$

In general, SVD is needed in each iteration of numerical methods for (3), which leads to high computational cost. To lower the computational cost, a matrix factorization method was considered by Xu *et al.*

[38], which preserves the low rank structure of matrix. Precisely, (2) is modeled as

$$\min_{X^i, Y^i, \mathcal{C}} \sum_{i=1}^3 \alpha_i \|X^i Y^i - C_{(i)}\|_F^2, \quad \text{s.t.} \quad P_{\Omega}(\mathcal{C}) = P_{\Omega}(\mathcal{M}). \quad (4)$$

This method has been widely used in various areas [24]. As pointed in [15, 16, 28], unfolding a tensor directly will destroy the original multi-way structure of the data, which leads to vital information loss and degraded performance. Note that the sizes of $C_{(i)}$, $i = 1, 2, 3$ in (4) are the same as \mathcal{C} in principle, which makes it difficult to lower the computational efforts.

Based on tubal rank, the following model was considered in [42] based on tensor factorization,

$$\min_{\mathcal{X}, \mathcal{Y}, \mathcal{C}} \frac{1}{2} \|\mathcal{X} * \mathcal{Y} - \mathcal{C}\|_F^2, \quad \text{s.t.} \quad P_{\Omega}(\mathcal{C} - \mathcal{M}) = 0, \quad (5)$$

where “*” denotes the t-product. By analysis in [15, 16, 28, 42], the t-product can be computed by some block diagonal matrices of smaller sizes, which makes a significant reduction of computational cost. Later, a corrected tensor nuclear norm minimization method was proposed in [39] for noisy observations.

It is valuable to mention that only one mode is considered in tubal rank and the other two modes are ignored. That is, low rank structure on the other two modes is missing. Motivated by this, we introduce a vector of tubal ranks on three different modes, called multi-tubal rank, which is similar to Tucker rank. Then a relationship between multi-tubal rank and Tucker rank is established. Based on the new introduced multi-tubal rank, a new tensor completion model is proposed. Similar to TCTF in [42], a tensor factorization based method is applied to solve the proposed model. In video and internet traffic tensor completion, spatio-temporal characteristics are intrinsic features. To make full use of such features, we improve the proposed low multi-tubal rank tensor completion model, and then apply tensor factorization based method for the improved model. To the best of authors’ knowledge, this paper is the first one to introduce multi-tubal rank, to present the relationship between tubal rank and Tucker rank and to introduce the spatio-temporal characteristics to recover video data. The reported numerical examples show that our results have less relative error and higher peak signal-to-noise ratio (PSNR) within less computational time than those of some existing methods. That is, our models and methods outperform the existing methods.

The paper is organized as follows. Section 2 introduces the multi-tubal rank of a third order tensor with motivation in both theory and application. In Section 3, a new model of tensor completion based on the multi-tubal rank is proposed and tensor factorization based method is applied with its corresponding convergence analysis. In Section 4, the tensor completion model is modified to tensor data with some characteristics when the involved data have spatio-temporal characteristics. For this improvement, tensor factorization based method is also modified. Finally, some numerical results on colorful image recovery, gray video recovery and internet traffic data recovery are reported, which show the efficiency of the proposed methods.

2 Multi-tubal rank: definition and motivation

Before proceeding, we present some notations here. For a positive integer n , $[\mathbf{n}] := \{1, 2, \dots, n\}$. Scalars, vectors and matrices are denoted as lowercase letters (a, b, c, \dots), boldface lowercase letters ($\mathbf{a}, \mathbf{b}, \mathbf{c}, \dots$)

and uppercase letters (A, B, C, \dots) , respectively. Third order tensors are denoted as $\mathcal{A}, \mathcal{B}, \mathcal{C}, \dots$, and the set of all the third order real tensors is denoted as $\mathbb{R}^{n_1 \times n_2 \times n_3}$. For a third order tensor \mathcal{A} , we use the Matlab notations $\mathcal{A}(i, :, :)$, $\mathcal{A}(:, j, :)$ and $\mathcal{A}(:, :, k)$ to denote its i -th horizontal, j -th lateral and k -th frontal slice, respectively. Let $\mathcal{A} = (\mathcal{A}_{ijk}) \in \mathbb{R}^{n_1 \times n_2 \times n_3}$, then $(A_1^{(i)})_{jk} = (A_2^{(j)})_{ik} = (A_3^{(k)})_{ij} = \mathcal{A}_{ijk}$ for all $i \in [\mathbf{n}_1]$, $j \in [\mathbf{n}_2]$ and $k \in [\mathbf{n}_3]$. The inner product of two tensors $\mathcal{A}, \mathcal{B} \in \mathbb{R}^{n_1 \times n_2 \times n_3}$ is the sum of products of their entries, i.e.

$$\langle \mathcal{A}, \mathcal{B} \rangle = \sum_{i=1}^{n_1} \sum_{j=1}^{n_2} \sum_{k=1}^{n_3} \mathcal{A}_{ijk} \mathcal{B}_{ijk}.$$

The Frobenius norm is $\|\mathcal{A}\|_F = \sqrt{\langle \mathcal{A}, \mathcal{A} \rangle}$. For a matrix A , A^* and A^{-1} represent the conjugate transpose and the inverse of A , respectively. I_n represents the identity matrix of size $n \times n$. For any $u \in [\mathbf{3}]$, the u -mode matrix product of a tensor $\mathcal{A} = (\mathcal{A}_{ijk}) \in \mathbb{R}^{n_1 \times n_2 \times n_3}$ with a matrix $M_u \in \mathbb{R}^{J \times n_u}$ is denoted by $\mathcal{A} \times_u M_u$ with its entries

$$\begin{aligned} (\mathcal{A} \times_1 M_1)_{ii_2 i_3} &= \sum_{i_1=1}^{n_1} \mathcal{A}_{i_1 i_2 i_3} (M_1)_{ii_1}, \\ (\mathcal{A} \times_2 M_2)_{i_1 j i_3} &= \sum_{i_2=1}^{n_2} \mathcal{A}_{i_1 i_2 i_3} (M_2)_{j i_2}, \\ (\mathcal{A} \times_3 M_3)_{i_1 i_2 k} &= \sum_{i_3=1}^{n_3} \mathcal{A}_{i_1 i_2 i_3} (M_3)_{k i_3}. \end{aligned}$$

2.1 Generalized T_u -product and multi-tubal rank

In this subsection, we will introduce multi-tubal rank, which is a generalization of tubal rank in [15]. Before proceeding, we review the Discrete Fourier Transformation (DFT), which plays a key role in tensor-tensor product (t-product). For $\mathcal{A} \in \mathbb{R}^{n_1 \times n_2 \times n_3}$ and $u \in [\mathbf{3}]$, let $\bar{\mathcal{A}}_u \in \mathbb{C}^{n_1 \times n_2 \times n_3}$ be the result of Discrete Fourier transformation (DFT) of $\mathcal{A} \in \mathbb{R}^{n_1 \times n_2 \times n_3}$ along the u -th mode. Specifically, let $F_{n_u} = [f_1, \dots, f_{n_u}] \in \mathbb{C}^{n_u \times n_u}$, where

$$f_i = \left[\omega^{0 \times (i-1)}; \omega^{1 \times (i-1)}; \dots; \omega^{(n_u-1) \times (i-1)} \right] \in \mathbb{C}^{n_u}$$

with $\omega = e^{-\frac{2\pi i}{n_u}}$ and $i = \sqrt{-1}$. Then

$$\bar{\mathcal{A}}_1(:, j, k) = F_{n_1} \mathcal{A}(:, j, k), \quad \bar{\mathcal{A}}_2(i, :, k) = F_{n_2} \mathcal{A}(i, :, k), \quad \bar{\mathcal{A}}_3(i, j, :) = F_{n_3} \mathcal{A}(i, j, :),$$

which can be computed by Matlab command “ $\bar{\mathcal{A}}_u = fft(\mathcal{A}, [], u)$ ”. Furthermore, \mathcal{A} can be computed by $\bar{\mathcal{A}}_u$ with the inverse DFT $\mathcal{A} = ifft(\bar{\mathcal{A}}_u, [], u)$.

For $\mathcal{A} \in \mathbb{R}^{n_1 \times n_2 \times n_3}$, we define matrices $\bar{A}_1 \in \mathbb{C}^{n_1 n_2 \times n_1 n_3}$, $\bar{A}_2 \in \mathbb{C}^{n_1 n_2 \times n_2 n_3}$ and $\bar{A}_3 \in \mathbb{C}^{n_1 n_3 \times n_2 n_3}$ as

$$\bar{A}_u = bdiag_u(\bar{\mathcal{A}}_u) = \begin{bmatrix} \bar{A}_u^{(1)} & & & \\ & \bar{A}_u^{(2)} & & \\ & & \ddots & \\ & & & \bar{A}_u^{(n_u)} \end{bmatrix}, \quad \forall u \in [\mathbf{3}]. \quad (6)$$

Here, $bdiag_u(\cdot)$ is an operator which maps the tensor $\bar{\mathcal{A}}_u$ to the block diagonal matrix \bar{A}_u . The block circulant matrices $bcirc_1(\mathcal{A}) \in \mathbb{R}^{n_1 n_2 \times n_1 n_3}$, $bcirc_2(\mathcal{A}) \in \mathbb{R}^{n_1 n_2 \times n_2 n_3}$ and $bcirc_3(\mathcal{A}) \in \mathbb{R}^{n_1 n_3 \times n_2 n_3}$ of \mathcal{A} are defined as

$$bcirc_u(\mathcal{A}) = \begin{bmatrix} A_u^{(1)} & A_u^{(n_u)} & \dots & A_u^{(2)} \\ A_u^{(2)} & A_u^{(1)} & \dots & A_u^{(3)} \\ \vdots & \vdots & \ddots & \vdots \\ A_u^{(n_u)} & A_u^{(n_u-1)} & \dots & A_u^{(1)} \end{bmatrix}, \quad \forall u \in [\mathbf{3}].$$

Based on these notations, the generalized T_u -product and multi-tubal rank are introduced as follows.

Definition 2.1 (Generalized T_u -product) For $\mathcal{A}_1 \in \mathbb{R}^{n_1 \times n_2 \times r_1}$ and $\mathcal{B}_1 \in \mathbb{R}^{n_1 \times r_1 \times n_3}$, define

$$\mathcal{A}_1 *_1 \mathcal{B}_1 := \text{fold}_1(\text{bcirc}_1(\mathcal{A}_1)) \cdot \text{unfold}_1(\mathcal{B}_1) \in \mathbb{R}^{n_1 \times n_2 \times n_3}.$$

For $\mathcal{A}_2 \in \mathbb{R}^{n_1 \times n_2 \times r_2}$ and $\mathcal{B}_2 \in \mathbb{R}^{r_2 \times n_2 \times n_3}$, define

$$\mathcal{A}_2 *_2 \mathcal{B}_2 := \text{fold}_2(\text{bcirc}_2(\mathcal{A}_2)) \cdot \text{unfold}_2(\mathcal{B}_2) \in \mathbb{R}^{n_1 \times n_2 \times n_3}.$$

For $\mathcal{A}_3 \in \mathbb{R}^{n_1 \times r_3 \times n_3}$ and $\mathcal{B}_3 \in \mathbb{R}^{r_3 \times n_2 \times n_3}$, define

$$\mathcal{A}_3 *_3 \mathcal{B}_3 := \text{fold}_3(\text{bcirc}_3(\mathcal{A}_3)) \cdot \text{unfold}_3(\mathcal{B}_3) \in \mathbb{R}^{n_1 \times n_2 \times n_3}.$$

Here

$$\text{unfold}_u(\mathcal{B}_u) = [B_u^{(1)}; B_u^{(2)}; \dots; B_u^{(n_u)}],$$

and its inverse operator “ fold_u ” is defined by $\text{fold}_u(\text{unfold}_u(\mathcal{B}_u)) = \mathcal{B}_u$.

Definition 2.2 (Multi-tubal rank) For any tensor $\mathcal{A} \in \mathbb{R}^{n_1 \times n_2 \times n_3}$ and $u \in [\mathbf{3}]$, let $r_u^l = \text{rank}(\bar{A}_u^{(l)})$ and $l \in [\mathbf{n}_u]$. Then multi-tubal rank of \mathcal{A} is defined as

$$\text{rank}_{mt}(\mathcal{A}) = (r_1(\mathcal{A}), r_2(\mathcal{A}), r_3(\mathcal{A})),$$

where $r_u(\mathcal{A}) = \max\{r_u^1, r_u^2, \dots, r_u^{n_u}\}$ for $u \in [\mathbf{3}]$.

In fact, the T_3 -product is the classical t -product and $r_3(\mathcal{A})$ is tubal rank [15] of tensor \mathcal{A} , respectively.

Lemma 2.1 [16] Suppose that \mathcal{A}, \mathcal{B} are tensors such that $\mathcal{F} := \mathcal{A} *_u \mathcal{B}$ ($u \in [\mathbf{3}]$) is well defined as in Definition 2.1. Let $\bar{A}_u, \bar{B}_u, \bar{F}_u$ be defined as in (6) and $r_u(\cdot)$ be defined as in Definition 2.2. Then

- (1). $\|\mathcal{A}\|_F^2 = \frac{1}{n_u} \|\bar{A}_u\|_F^2$;
- (2). $\mathcal{F} = \mathcal{A} *_u \mathcal{B}$ and $\bar{F}_u = \bar{A}_u \bar{B}_u$ are equivalent;
- (3). $r_u(\mathcal{F}) \leq \min\{r_u(\mathcal{A}), r_u(\mathcal{B})\}$.

From Lemma 2.1, we can assert that the generalized tensor factorization can be computed by matrix factorization, which is computable.

2.2 Motivation of multi-tubal rank

We first discuss the relationship between Tucker rank and multi-tubal rank. To this end, we need the following lemma.

Lemma 2.2 Suppose that $\mathcal{C} \in \mathbb{R}^{n_1 \times n_2 \times n_3}$, $F \in \mathbb{R}^{n_1 \times n_1}$, $G \in \mathbb{R}^{n_2 \times n_2}$ and $H \in \mathbb{R}^{n_3 \times n_3}$. Let $\mathcal{F} \in \mathbb{R}^{n_1 \times n_2 \times n_1}$, $\tilde{\mathcal{F}} \in \mathbb{R}^{n_1 \times n_1 \times n_3}$, $\mathcal{G} \in \mathbb{R}^{n_2 \times n_2 \times n_3}$, $\tilde{\mathcal{G}} \in \mathbb{R}^{n_1 \times n_2 \times n_2}$, $\mathcal{H} \in \mathbb{R}^{n_1 \times n_3 \times n_3}$, $\tilde{\mathcal{H}} \in \mathbb{R}^{n_3 \times n_2 \times n_3}$ be the tensors with their slices

$$\begin{aligned} F_2^{(1)} &= F, F_2^{(2)} = \dots = F_2^{(n_2)} = 0, & \tilde{F}_3^{(1)} &= F, \tilde{F}_3^{(2)} = \dots = \tilde{F}_3^{(n_3)} = 0, \\ G_3^{(1)} &= G^T, G_3^{(2)} = \dots = G_3^{(n_3)} = 0, & \tilde{G}_1^{(1)} &= G, \tilde{G}_1^{(2)} = \dots = \tilde{G}_1^{(n_1)} = 0, \\ H_1^{(1)} &= H^T, H_1^{(2)} = \dots = H_1^{(n_1)} = 0, & \tilde{H}_2^{(1)} &= H^T, \tilde{H}_2^{(2)} = \dots = \tilde{H}_2^{(n_2)} = 0. \end{aligned}$$

Then

$$\begin{cases} \mathcal{F} *_2 \mathcal{C} = \mathcal{C} \times_1 F, \\ \tilde{\mathcal{F}} *_3 \mathcal{C} = \mathcal{C} \times_1 F, \end{cases} \quad \begin{cases} \mathcal{C} *_3 \mathcal{G} = \mathcal{C} \times_2 G, \\ \tilde{\mathcal{G}} *_1 \mathcal{C} = \mathcal{C} \times_2 G, \end{cases} \quad \begin{cases} \mathcal{C} *_1 \mathcal{H} = \mathcal{C} \times_3 H, \\ \mathcal{C} *_2 \tilde{\mathcal{H}} = \mathcal{C} \times_3 H. \end{cases}$$

Proof. It clear to see that

$$\begin{aligned} \text{unfold}_2(\mathcal{F} *_2 \mathcal{C}) &= \text{bcirc}_2(\mathcal{F}) \cdot \text{unfold}_2(\mathcal{C}) \\ &= \begin{bmatrix} F_2^{(1)} & F_2^{(n_2)} & \dots & F_2^{(2)} \\ F_2^{(2)} & F_2^{(1)} & \dots & F_2^{(3)} \\ \vdots & \vdots & \ddots & \vdots \\ F_2^{(n_2)} & F_2^{(n_2-1)} & \dots & F_2^{(1)} \end{bmatrix} \begin{bmatrix} C_2^{(1)} \\ C_2^{(2)} \\ \vdots \\ C_2^{(n_2)} \end{bmatrix} \\ &= \begin{bmatrix} F & 0 & \dots & 0 \\ 0 & F & \dots & 0 \\ \vdots & \vdots & \ddots & \vdots \\ 0 & 0 & \dots & F \end{bmatrix} \begin{bmatrix} C_2^{(1)} \\ C_2^{(2)} \\ \vdots \\ C_2^{(n_2)} \end{bmatrix} = \begin{bmatrix} FC_2^{(1)} \\ FC_2^{(2)} \\ \vdots \\ FC_2^{(n_2)} \end{bmatrix}. \end{aligned}$$

Then

$$(\mathcal{F} *_2 \mathcal{C})_{ijk} = (FC_2^{(j)})_{ik} = \sum_{p=1}^{n_1} F_{ip} (C_2^{(j)})_{pk} = \sum_{p=1}^{n_1} C_{pjk} F_{ip} = (\mathcal{C} \times_1 F)_{ijk}.$$

Similarly,

$$(\tilde{\mathcal{F}} *_3 \mathcal{C})_{ijk} = (FC_3^{(k)})_{ij} = \sum_{p=1}^{n_1} F_{ip} (C_3^{(k)})_{pj} = \sum_{p=1}^{n_1} C_{pjk} F_{ip} = (\mathcal{C} \times_1 F)_{ijk}.$$

Now we can assert that $\mathcal{F} *_2 \mathcal{C} = \mathcal{C} \times_1 F$ and $\tilde{\mathcal{F}} *_3 \mathcal{C} = \mathcal{C} \times_1 F$.

Furthermore,

$$\begin{aligned} \text{unfold}_3(\mathcal{C} *_3 \mathcal{G}) &= \text{bcirc}_3(\mathcal{C}) \cdot \text{unfold}_3(\mathcal{G}) \\ &= \begin{bmatrix} C_3^{(1)} & C_3^{(n_3)} & \dots & C_3^{(2)} \\ C_3^{(2)} & C_3^{(1)} & \dots & C_3^{(3)} \\ \vdots & \vdots & \ddots & \vdots \\ C_3^{(n_3)} & C_3^{(n_3-1)} & \dots & C_3^{(1)} \end{bmatrix} \begin{bmatrix} G_3^{(1)} \\ G_3^{(2)} \\ \vdots \\ G_3^{(n_3)} \end{bmatrix} \\ &= \begin{bmatrix} C_3^{(1)} & C_3^{(n_3)} & \dots & C_3^{(2)} \\ C_3^{(2)} & C_3^{(1)} & \dots & C_3^{(3)} \\ \vdots & \vdots & \ddots & \vdots \\ C_3^{(n_3)} & C_3^{(n_3-1)} & \dots & C_3^{(1)} \end{bmatrix} \begin{bmatrix} G^T \\ 0 \\ \vdots \\ 0 \end{bmatrix} = \begin{bmatrix} C_3^{(1)} G^T \\ C_3^{(2)} G^T \\ \vdots \\ C_3^{(n_3)} G^T \end{bmatrix}. \end{aligned}$$

Then

$$(\mathcal{C} *_3 \mathcal{G})_{ijk} = \left(C_3^{(k)} G^T \right)_{ij} = \sum_{p=1}^{n_2} \left(C_3^{(k)} \right)_{ip} (G^T)_{pj} = \sum_{p=1}^{n_2} \mathcal{C}_{ipk} G_{jp} = (\mathcal{C} \times_2 G)_{ijk}.$$

Similarly,

$$\left(\tilde{\mathcal{G}} *_1 \mathcal{C} \right)_{ijk} = \left(G C_1^{(i)} \right)_{jk} = \sum_{p=1}^{n_2} (G)_{jp} \left(C_1^{(i)} \right)_{pk} = \sum_{p=1}^{n_2} \mathcal{C}_{ipk} G_{jp} = (\mathcal{C} \times_2 G)_{ijk}.$$

Then $\mathcal{C} *_3 \mathcal{G} = \mathcal{C} \times_2 G$ and $\tilde{\mathcal{G}} *_1 \mathcal{C} = \mathcal{C} \times_2 G$. Similarly, $\mathcal{C} *_1 \mathcal{H} = \mathcal{C} \times_3 H$ and $\mathcal{C} *_2 \tilde{\mathcal{H}} = \mathcal{C} \times_3 H$. Hence the desired results are arrived. \blacksquare

Theorem 2.1 For any tensor $\mathcal{A} = (\mathcal{A}_{ijk}) \in \mathbb{R}^{n_1 \times n_2 \times n_3}$, the following properties hold:

$$\begin{aligned} r_1(\mathcal{A}) &\leq \min \{ r(A_{(2)}), r(A_{(3)}) \}, \quad r_2(\mathcal{A}) \leq \min \{ r(A_{(1)}), r(A_{(3)}) \}, \\ r_3(\mathcal{A}) &\leq \min \{ r(A_{(1)}), r(A_{(2)}) \}. \end{aligned}$$

Proof. Let $\mathcal{A} = \mathcal{B} \times_1 U^{(1)} \times_2 U^{(2)} \times_3 U^{(3)}$ be a Tucker rank decomposition of \mathcal{A} , then $r(A_{(3)}) = r(U^{(3)})$ and $\mathcal{A} = \tilde{\mathcal{B}} \times_3 U^{(3)}$, where $\tilde{\mathcal{B}} = \mathcal{B} \times_1 U^{(1)} \times_2 U^{(2)}$. By Lemma 2.2, we have $\mathcal{A} = \tilde{\mathcal{B}} \times_3 U^{(3)} = \tilde{\mathcal{B}} *_1 \mathcal{U}$, where $\mathcal{U} \in \mathbb{R}^{n_1 \times n_3 \times n_3}$ with its slices

$$U_1^{(1)} = \left(U^{(3)} \right)^T, \quad U_1^{(2)} = \dots = U_1^{(n_1)} = 0.$$

Denote $\bar{\mathcal{U}}_1 = \text{fft}(\mathcal{U}, [], 1)$, then $\bar{\mathcal{U}}_1(:, j, k) = F_{n_1} \mathcal{U}(:, j, k)$, then

$$\bar{\mathcal{U}}_1(i, :, :) = \sum_{l=1}^{n_1} F_{n_1}(i, l) \mathcal{U}(l, :, :) = F_{n_1}(i, 1) \left(U^{(3)} \right)^T, \quad \forall i \in [n_1].$$

From the definition of F_{n_1} , $F_{n_1}(1, i) \neq 0$. Thus $r_1(\mathcal{U}) = r(U^{(3)})$. From Lemma 2.1 and $\mathcal{A} = \tilde{\mathcal{B}} *_1 \mathcal{U}$, we have

$$r_1(\mathcal{A}) \leq r_1(\mathcal{U}) = r(U^{(3)}) = r(A_{(3)}).$$

Similarly, $r_1(\mathcal{A}) \leq r(A_{(2)})$. Now we can assert that $r_1(\mathcal{A}) \leq \min \{ r(A_{(2)}), r(A_{(3)}) \}$. Similarly,

$$r_2(\mathcal{A}) \leq \min \{ r(A_{(1)}), r(A_{(3)}) \}, \quad r_3(\mathcal{A}) \leq \min \{ r(A_{(1)}), r(A_{(2)}) \},$$

which show the desired results. \blacksquare

Low Tucker rank tensor completion model were considered in various references. Note that Tucker rank considers low rank structures on all modes of tensor, while only one low rank structure in tubal rank is considered, which leads to low rank structures on the other two modes missed. To consider low rank structures on all the three modes of tensor, it is necessary to consider multi-tubal rank in tensor completion problem.

Now we take the video tensor data in real world for example to see the low rank structures of tensors. In video tensor¹, there are two spatial dimensions and one temporal dimension. We take the first 30 frames of size 144×176 as a video tensor \mathcal{A} , that is $\mathcal{A} \in \mathbb{R}^{144 \times 176 \times 30}$. Figure 1 (a) shows the sampled frames in the video. Figure 1 (b) shows the first 30 singular values of the matrix $\bar{A}_3^{(1)}$. Apply SVD to $\bar{A}_1^{(1)}$ and $\bar{A}_2^{(1)}$ to obtain their singular values, shown in Figure 1 (c) and Figure 1 (d), respectively. From Figure 1 (c) and (d), the low rank structures of tensor \mathcal{A} on mode 1 and mode 2 are presented.

¹<http://trace.eas.asu.edu/yuv/>

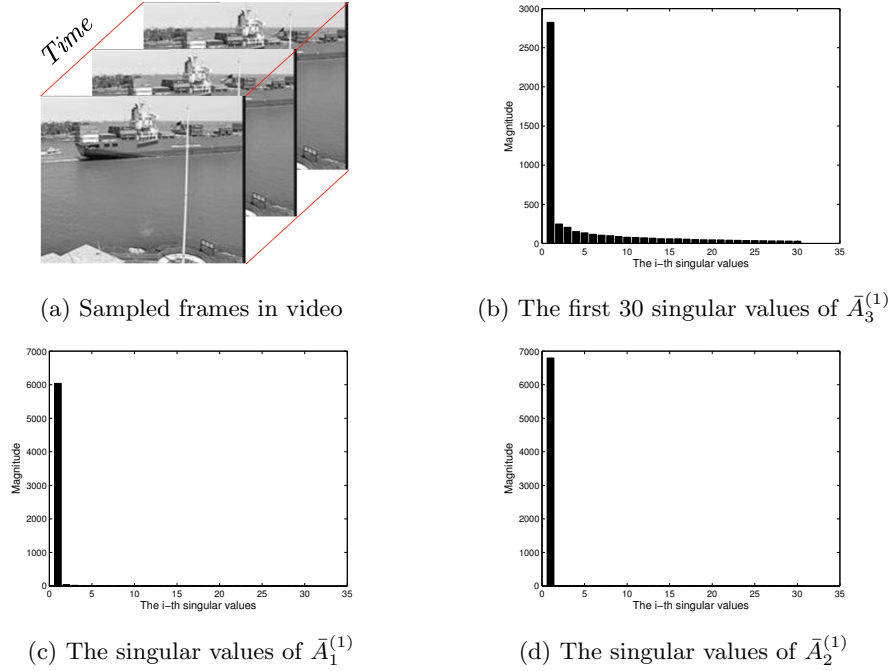


Figure 1: The sampled frames in video and singular values of $\bar{A}_u^{(1)}$ for $u \in [3]$

Motivated by this, we introduce multi-tubal rank, which is similar to Tucker rank. The introduced multi-tubal rank includes low rank structures on all three modes of third order tensor, which take full considerations of all low rank structures and will lead to promising performance for solving tensor completion problem.

3 Tensor completion problem based on multi-tubal rank

In this section, we establish a low rank tensor completion based on multi-tubal rank and then apply a tensor factorization based method for solving it. For the method, the convergence analysis will be presented.

3.1 Tensor completion model based on multi-tubal rank and its tensor factorization based method

Based on the introduced multi-tubal rank, the tensor completion problem can be modeled as

$$\min_{\mathcal{C} \in \mathbb{R}^{n_1 \times n_2 \times n_3}} \text{rank}_{mt}(\mathcal{C}), \quad \text{s.t.} \quad P_{\Omega}(\mathcal{C} - \mathcal{M}) = 0, \quad (7)$$

which is a vector optimization problem. To keep things simple, we consider the weighted multi-tubal rank minimization problem as

$$\min_{\mathcal{C} \in \mathbb{R}^{n_1 \times n_2 \times n_3}} \sum_{u=1}^3 \alpha_u r_u(\mathcal{C}), \quad \text{s.t.} \quad P_{\Omega}(\mathcal{C} - \mathcal{M}) = 0,$$

where $\alpha_1, \alpha_2, \alpha_3 \geq 0$ and $\sum_{u=1}^3 \alpha_u = 1$. Note that \mathcal{C} can be factorized as $\mathcal{C} = \mathcal{X}_u *_{\mathcal{U}} \mathcal{Y}_u$ with $r_u(\mathcal{C}) \leq \min(r_u(\mathcal{X}_u), r_u(\mathcal{Y}_u))$ for $u \in [3]$. Hence we consider the following tensor factorization model

$$\min_{\mathcal{C}, \mathcal{X}_u, \mathcal{Y}_u} \sum_{u=1}^3 \frac{\alpha_u}{2} \|\mathcal{X}_u *_{\mathcal{U}} \mathcal{Y}_u - \mathcal{C}\|_F^2, \quad \text{s.t.} \quad P_{\Omega}(\mathcal{C} - \mathcal{M}) = 0. \quad (8)$$

To solve problem (8) more conveniently, we introduce its regularized model as follows:

$$\min_{\mathcal{C}, \mathcal{X}_u, \mathcal{Y}_u} f(\mathcal{C}, \mathcal{X}_1, \mathcal{X}_2, \mathcal{X}_3, \mathcal{Y}_1, \mathcal{Y}_2, \mathcal{Y}_3), \quad \text{s.t.} \quad P_{\Omega}(\mathcal{C} - \mathcal{M}) = 0. \quad (9)$$

Here,

$$f(\mathcal{C}, \mathcal{X}_1, \mathcal{X}_2, \mathcal{X}_3, \mathcal{Y}_1, \mathcal{Y}_2, \mathcal{Y}_3) = \sum_{u=1}^3 \left(\frac{\alpha_u}{2} \|\mathcal{X}_u *_{\mathcal{U}} \mathcal{Y}_u - \mathcal{C}\|_F^2 + \frac{\lambda}{2} (\|\mathcal{X}_u\|_F^2 + \|\mathcal{Y}_u\|_F^2) \right). \quad (10)$$

Now, we are ready to update \mathcal{C} , \mathcal{X}_u and \mathcal{Y}_u for all $u \in [3]$. Note that

$$\begin{aligned} & \sum_{u=1}^3 \alpha_u \|\mathcal{X}_u *_{\mathcal{U}} \mathcal{Y}_u - \mathcal{C}\|_F^2 = \sum_{u=1}^3 \alpha_u \langle \mathcal{X}_u *_{\mathcal{U}} \mathcal{Y}_u - \mathcal{C}, \mathcal{X}_u *_{\mathcal{U}} \mathcal{Y}_u - \mathcal{C} \rangle \\ &= \sum_{u=1}^3 \alpha_u \langle \mathcal{C}, \mathcal{C} \rangle - 2 \sum_{u=1}^3 \alpha_u \langle \mathcal{X}_u *_{\mathcal{U}} \mathcal{Y}_u, \mathcal{C} \rangle + \sum_{u=1}^3 \alpha_u \langle \mathcal{X}_u *_{\mathcal{U}} \mathcal{Y}_u, \mathcal{X}_u *_{\mathcal{U}} \mathcal{Y}_u \rangle \\ &= \langle \mathcal{C}, \mathcal{C} \rangle - 2 \left\langle \sum_{u=1}^3 \alpha_u \mathcal{X}_u *_{\mathcal{U}} \mathcal{Y}_u, \mathcal{C} \right\rangle + \sum_{u=1}^3 \alpha_u \|\mathcal{X}_u *_{\mathcal{U}} \mathcal{Y}_u\|_F^2 \\ &= \left\langle \sum_{u=1}^3 \alpha_u \mathcal{X}_u *_{\mathcal{U}} \mathcal{Y}_u - \mathcal{C}, \sum_{u=1}^3 \alpha_u \mathcal{X}_u *_{\mathcal{U}} \mathcal{Y}_u - \mathcal{C} \right\rangle + \sum_{u=1}^3 \alpha_u \|\mathcal{X}_u *_{\mathcal{U}} \mathcal{Y}_u\|_F^2 - \left\| \sum_{u=1}^3 \alpha_u \mathcal{X}_u *_{\mathcal{U}} \mathcal{Y}_u \right\|_F^2 \\ &= \left\| \sum_{u=1}^3 \alpha_u \mathcal{X}_u *_{\mathcal{U}} \mathcal{Y}_u - \mathcal{C} \right\|_F^2 + \sum_{u=1}^3 \alpha_u \|\mathcal{X}_u *_{\mathcal{U}} \mathcal{Y}_u\|_F^2 - \left\| \sum_{u=1}^3 \alpha_u \mathcal{X}_u *_{\mathcal{U}} \mathcal{Y}_u \right\|_F^2. \end{aligned} \quad (11)$$

Then \mathcal{C}^{t+1} can be updated by

$$\mathcal{C}^{t+1} = \underset{P_{\Omega}(\mathcal{C} - \mathcal{M})=0}{\operatorname{argmin}} \frac{1}{2} \left\| \sum_{u=1}^3 \alpha_u \mathcal{X}_u^t *_{\mathcal{U}} \mathcal{Y}_u^t - \mathcal{C} \right\|_F^2 = \sum_{u=1}^3 \alpha_u \mathcal{X}_u^t *_{\mathcal{U}} \mathcal{Y}_u^t + P_{\Omega} \left(\mathcal{M} - \sum_{u=1}^3 \alpha_u \mathcal{X}_u^t *_{\mathcal{U}} \mathcal{Y}_u^t \right). \quad (12)$$

Before we present how to update \mathcal{X}_u^{t+1} and \mathcal{Y}_u^{t+1} , we rewrite (9) as a corresponding matrix version. Denote $r_u := r_u(\mathcal{C})$, $r_u^l := r_u^l(\bar{\mathcal{C}}_u^{(l)})$ with $\bar{\mathcal{C}}_u^{(l)} \in \mathbb{C}^{n_{u_1} \times n_{u_2}}$, $u_1 < u_2$ and $u_1, u_2 \neq u$. Clearly, $r_u^l \leq r_u$ for all $l \in [\mathbf{n}_u]$. For each u and l , $\bar{\mathcal{C}}_u^{(l)}$ can be factorized as a product of two matrices $\hat{X}_u^{(l)}$ and $\hat{Y}_u^{(l)}$ of smaller sizes, where $\hat{X}_u^{(l)} \in \mathbb{C}^{n_{u_1} \times r_u^l}$ and $\hat{Y}_u^{(l)} \in \mathbb{C}^{r_u^l \times n_{u_2}}$ are the l th block diagonal matrices of $\hat{X}_u \in \mathbb{C}^{n_{u_1} n_u \times (\sum_{l=1}^{n_u} r_u^l)}$ and $\hat{Y}_u \in \mathbb{C}^{(\sum_{l=1}^{n_u} r_u^l) \times n_u n_{u_2}}$. Let $\bar{X}_u^{(l)} = [\hat{X}_u^{(l)}, 0] \in \mathbb{C}^{n_{u_1} \times r_u}$, $\bar{Y}_u^{(l)} = [\hat{Y}_u^{(l)}; 0] \in \mathbb{C}^{r_u \times n_{u_2}}$ and \bar{X}_u, \bar{Y}_u be the block diagonal matrices with the l th block diagonal matrices $\bar{X}_u^{(l)}, \bar{Y}_u^{(l)}$, respectively. Then $\hat{X}_u \hat{Y}_u = \bar{X}_u \bar{Y}_u$. Together with Lemma 2.1, we have

$$\|\mathcal{X}_u *_{\mathcal{U}} \mathcal{Y}_u - \mathcal{C}\|_F^2 = \frac{1}{n_u} \|\bar{X}_u \bar{Y}_u - \bar{\mathcal{C}}_u\|_F^2 = \frac{1}{n_u} \|\hat{X}_u \hat{Y}_u - \bar{\mathcal{C}}_u\|_F^2 = \frac{1}{n_u} \sum_{l=1}^{n_u} \|\hat{X}_u^{(l)} \hat{Y}_u^{(l)} - \bar{\mathcal{C}}_u^{(l)}\|_F^2, \quad u \in [3].$$

Therefore, (9) can be rewritten as

$$\begin{aligned} & \min_{\mathcal{C}, \mathcal{X}_u, \mathcal{Y}_u} \sum_{u=1}^3 \sum_{l=1}^{n_u} \left(\frac{\alpha_u}{2n_u} \left\| \hat{X}_u^{(l)} \hat{Y}_u^{(l)} - \bar{\mathcal{C}}_u^{(l)} \right\|_F^2 \right) + \sum_{u=1}^3 \sum_{l=1}^{n_u} \left(\frac{\lambda}{2n_u} \left\| \hat{X}_u^{(l)} \right\|_F^2 + \frac{\lambda}{2n_u} \left\| \hat{Y}_u^{(l)} \right\|_F^2 \right) \\ & \text{s.t.} \quad P_{\Omega}(\mathcal{C} - \mathcal{M}) = 0. \end{aligned} \quad (13)$$

To update $\hat{X}_u^{(l,t)}$, we consider its regularized version and have $\hat{X}_u^{(l,t+1)}$ as follows.

$$\begin{aligned}\hat{X}_u^{(l,t+1)} &= \underset{\hat{X}_u^{(l)}}{\operatorname{argmin}} \frac{\alpha_u}{2n_u} \left\| \hat{X}_u^{(l)} \hat{Y}_u^{(l,t)} - \bar{C}_u^{(l,t+1)} \right\|_F^2 + \frac{\lambda}{2n_u} \left(\left\| \hat{X}_u^{(l)} \right\|_F^2 + \left\| \hat{X}_u^{(l)} - \hat{X}_u^{(l,t)} \right\|_F^2 \right) \\ &= \left(\lambda \hat{X}_u^{(l,t)} + \alpha_u \bar{C}_u^{(l,t+1)} \left(\hat{Y}_u^{(l,t)} \right)^* \right) \left(\alpha_u \hat{Y}_u^{(l,t)} \left(\hat{Y}_u^{(l,t)} \right)^* + 2\lambda I \right)^{-1}, \forall u \in [\mathbf{3}], \forall l \in [\mathbf{n}_u].\end{aligned}\quad (14)$$

Similarly, $\hat{Y}_u^{(l,t+1)}$ can be updated by

$$\begin{aligned}\hat{Y}_u^{(l,t+1)} &= \underset{\hat{Y}_u^{(l)}}{\operatorname{argmin}} \frac{\alpha_u}{2n_u} \left\| \hat{X}_u^{(l,t+1)} \hat{Y}_u^{(l)} - \bar{C}_u^{(l,t+1)} \right\|_F^2 + \frac{\lambda}{2n_u} \left(\left\| \hat{Y}_u^{(l)} \right\|_F^2 + \left\| \hat{Y}_u^{(l)} - \hat{Y}_u^{(l,t)} \right\|_F^2 \right) \\ &= \left(\alpha_u \left(\hat{X}_u^{(l,t+1)} \right)^* \hat{X}_u^{(l,t+1)} + 2\lambda I \right)^{-1} \left(\lambda \hat{Y}_u^{(l,t)} + \alpha_u \left(\hat{X}_u^{(l,t+1)} \right)^* \bar{C}_u^{(l,t+1)} \right), \forall u \in [\mathbf{3}], \forall l \in [\mathbf{n}_u].\end{aligned}\quad (15)$$

Based on above discussions, a tensor factorization algorithm can be outlined as Algorithm 3.1, denoted by MTRTC.

Algorithm 3.1 Multi-Tubal Rank Tensor Completion (MTRTC)

Input: The tensor data $\mathcal{M} \in \mathbb{R}^{n_1 \times n_2 \times n_3}$, the observed set Ω , the initialized rank R^0 , parameters λ , ε and α_u , $u \in [\mathbf{3}]$.

Initialization: $\hat{X}_u^0, \hat{Y}_u^0, u \in [\mathbf{3}]$.

While not converge do

1. Fix \hat{X}_u^t and \hat{Y}_u^t to compute \mathcal{C}^{t+1} by (12).
2. Fix \hat{Y}_u^t and \mathcal{C}^{t+1} to update \hat{X}_u^{t+1} by (14).
3. Fix \hat{X}_u^{t+1} and \mathcal{C}^{t+1} to update \hat{Y}_u^{t+1} by (15).
4. Adopt the rank decreasing scheme to adjust $\operatorname{rank}_{mt}(\mathcal{C})$ and adjust the sizes of \hat{X}_u^{t+1} and \hat{Y}_u^{t+1} .
5. Check the stop criterion: $\|\mathcal{C}_\Omega^{t+1} - \mathcal{M}_\Omega\|_F / \|\mathcal{M}_\Omega\|_F < \varepsilon$.
6. $t \leftarrow t + 1$.

end while

Output: \mathcal{C}^{t+1} .

Remark 3.1 In general, we do not know the true multi-tubal rank of optimal tensor \mathcal{C} in advance. Thus, it is necessary to estimate the multi-tubal rank of tensor \mathcal{C} . In this paper, we adopt the same rank estimation and rank decreasing strategy proposed in [37, 38, 42].

3.2 Convergence analysis

In this subsection, we present the convergence of MTRTC. The following notation will be used in our analysis. In problem (9), Ω is an index set which locates the observed data. We use Ω^c to denote the complement of the set Ω with respect to the set $\{(i, j, k) : i \in [\mathbf{n}_1], j \in [\mathbf{n}_2], k \in [\mathbf{n}_3]\}$. To simply the notation, we denote $z^t = (\mathcal{C}^t, \mathcal{X}_1^t, \mathcal{X}_2^t, \mathcal{X}_3^t, \mathcal{Y}_1^t, \mathcal{Y}_2^t, \mathcal{Y}_3^t)$ in this subsection.

Before proceeding, we present the Kurdyka-Lojasiewicz (KL) property [3] with constraint defined as below.

Definition 3.1 (Kurdyka-Lojasiewicz (KL) property) *Let Z be an open set and $f : Z \rightarrow \mathbb{R}$ be a semi-algebra function. For every critical point $z^* \in Z$ of f , there are a neighborhood of z^* , denoted by $Z' \subset Z$, an exponent $\theta \in [0, 1)$ and a positive constant μ such that*

$$|f(z) - f(z^*)|^\theta \leq \mu \left\| \prod_{\Omega} (\nabla f(z)) \right\|_F \quad (16)$$

for all $z \in Z'$, where $\prod_{\Omega}(\nabla f(z))$ denotes the projective gradient of f .

Recall that $f(z)$ defined as in (10), $f(z)$ is a quadratic function on z , and hence is a semi-algebra function. From Definition (3.1), for any critical point z^* , there exist θ and μ such that (16) is satisfied.

Theorem 3.1 *Suppose that $\{z^t\}$ is an infinite sequence generated by MTRTC. Then we have the following statements.*

- (1). *The sequence $\{z^t\}$ is bounded and any accumulation point of $\{z^t\}$ is a stationary point of problem (10).*
- (2). *There is a constant $\eta > 0$ such that $\eta \|z^t - z^{t+1}\|_F \geq \|\prod_{\Omega}(\nabla f(z^t))\|_F$.*

Proof. Since rank $r \geq 0$ in Algorithm MTRTC is non-increasing, we can assume that the rank r is fixed for all z^t when t is sufficiently large. That is, the rank decreasing scheme is not adopted for all such big enough t . For simplicity, we assume that t is big enough such that r is fixed and denote $f^t = f(z^t)$ in the following.

(1). By (12), it follows

$$\begin{aligned} \|C^{t+1} - C^t\|_F^2 &= \left\| \sum_{u=1}^3 \alpha_u \mathcal{X}_u^t *_{*u} \mathcal{Y}_u^t + P_{\Omega} \left(\mathcal{M} - \sum_{u=1}^3 \alpha_u \mathcal{X}_u^t *_{*u} \mathcal{Y}_u^t \right) - C^t \right\|_F^2 \\ &= \left\| \sum_{u=1}^3 \alpha_u \mathcal{X}_u^t *_{*u} \mathcal{Y}_u^t - C^t + P_{\Omega} \left(\mathcal{M} - \sum_{u=1}^3 \alpha_u \mathcal{X}_u^t *_{*u} \mathcal{Y}_u^t \right) \right\|_F^2 \\ &= \left\| \left(\sum_{u=1}^3 \alpha_u \mathcal{X}_u^t *_{*u} \mathcal{Y}_u^t - C^t \right) \right\|_{\Omega^c}^2. \end{aligned}$$

According to Algorithm MTRTC, we have that

$$\begin{aligned}
f^t - f^{t+1} &= \sum_{u=1}^3 \left(\frac{\alpha_u}{2} \|\mathcal{X}_u^t *_u \mathcal{Y}_u^t - \mathcal{C}^t\|_F^2 + \frac{\lambda}{2} \left(\|\mathcal{X}_u^t\|_F^2 + \|\mathcal{Y}_u^t\|_F^2 \right) \right) \\
&\quad - \sum_{u=1}^3 \left(\frac{\alpha_u}{2} \|\mathcal{X}_u^{t+1} *_u \mathcal{Y}_u^{t+1} - \mathcal{C}^{t+1}\|_F^2 + \frac{\lambda}{2} \left(\|\mathcal{X}_u^{t+1}\|_F^2 + \|\mathcal{Y}_u^{t+1}\|_F^2 \right) \right) \\
&= \sum_{u=1}^3 \frac{\alpha_u}{2} \left(\|\mathcal{X}_u^t *_u \mathcal{Y}_u^t - \mathcal{C}^t\|_F^2 - \|\mathcal{X}_u^t *_u \mathcal{Y}_u^t - \mathcal{C}^{t+1}\|_F^2 \right) \\
&\quad + \sum_{u=1}^3 \frac{\alpha_u}{2} \left(\|\mathcal{X}_u^t *_u \mathcal{Y}_u^t - \mathcal{C}^{t+1}\|_F^2 - \|\mathcal{X}_u^{t+1} *_u \mathcal{Y}_u^t - \mathcal{C}^{t+1}\|_F^2 \right) + \sum_{u=1}^3 \frac{\lambda}{2} \left(\|\mathcal{X}_u^t\|_F^2 - \|\mathcal{X}_u^{t+1}\|_F^2 \right) \\
&\quad + \sum_{u=1}^3 \frac{\alpha_u}{2} \left(\|\mathcal{X}_u^{t+1} *_u \mathcal{Y}_u^t - \mathcal{C}^{t+1}\|_F^2 - \|\mathcal{X}_u^{t+1} *_u \mathcal{Y}_u^{t+1} - \mathcal{C}^{t+1}\|_F^2 \right) + \sum_{u=1}^3 \frac{\lambda}{2} \left(\|\mathcal{Y}_u^t\|_F^2 - \|\mathcal{Y}_u^{t+1}\|_F^2 \right) \\
&\geq \frac{1}{2} \left(\left\| \sum_{u=1}^3 \alpha_u \mathcal{X}_u^t *_u \mathcal{Y}_u^t - \mathcal{C}^t \right\|_F^2 - \left\| \sum_{u=1}^3 \alpha_u \mathcal{X}_u^t *_u \mathcal{Y}_u^t - \mathcal{C}^{t+1} \right\|_F^2 \right) \\
&\quad + \sum_{u=1}^3 \sum_{l=1}^{n_u} \frac{\lambda}{2n_u} \left(\left\| \hat{X}_u^{(l,t)} - \hat{X}_u^{(l,t+1)} \right\|_F^2 + \left\| \hat{Y}_u^{(l,t)} - \hat{Y}_u^{(l,t+1)} \right\|_F^2 \right) \\
&= \frac{1}{2} \left\| \left(\sum_{u=1}^3 \alpha_u \mathcal{X}_u^t *_u \mathcal{Y}_u^t - \mathcal{C}^t \right) \right\|_{\Omega^c}^2 + \frac{\lambda}{2} \sum_{u=1}^3 \left(\|\mathcal{X}_u^t - \mathcal{X}_u^{t+1}\|_F^2 + \|\mathcal{Y}_u^t - \mathcal{Y}_u^{t+1}\|_F^2 \right) \\
&= \frac{1}{2} \|\mathcal{C}^{t+1} - \mathcal{C}^t\|_F^2 + \frac{\lambda}{2} \sum_{u=1}^3 \left(\|\mathcal{X}_u^t - \mathcal{X}_u^{t+1}\|_F^2 + \|\mathcal{Y}_u^t - \mathcal{Y}_u^{t+1}\|_F^2 \right) \\
&\geq \frac{\min\{1, \lambda\}}{2} \|z^{t+1} - z^t\|_F^2,
\end{aligned} \tag{17}$$

where the first inequality holds from (12), (14) and (15). Therefore, $\{f^t\}$ is monotonically decreasing. Together with the fact that $f \geq 0$, the series $\sum_{t=1}^{\infty} (f^t - f^{t+1}) = f^1 - \lim_{t \rightarrow \infty} f^t$ converges. Hence,

$$\sum_{t=1}^{\infty} (f^t - f^{t+1}) < \infty, \quad \sum_{t=1}^{\infty} (\mathcal{C}^{t+1} - \mathcal{C}^t) < \infty, \quad \sum_{t=1}^{\infty} \|z^t - z^{t+1}\|_F^2 < \infty.$$

Since $f^t \geq \sum_{u=1}^3 \frac{\lambda}{2n_u} \left(\|\hat{X}_u^t\|_F^2 + \|\hat{Y}_u^t\|_F^2 \right) = \frac{\lambda}{2} \sum_{u=1}^3 \left(\|\mathcal{X}_u^t\|_F^2 + \|\mathcal{Y}_u^t\|_F^2 \right)$, $\{\mathcal{X}_u^t\}$, $\{\mathcal{Y}_u^t\}$ are bounded. Together with the expression of \mathcal{C}^t , it is asserted that $\{\mathcal{C}^t\}$ is also bounded, and hence $\{z^t\}$ is bounded.

Clearly, there exists a convergent subsequence of $\{z^t\}$. Without loss of generality, we assume that $\lim_{k \rightarrow \infty} z^{t_k} = z^*$. From $\sum_{t=1}^{\infty} \|z^t - z^{t+1}\|_F^2 < \infty$, $\lim_{t \rightarrow \infty} z^{t+1} - z^t = 0$, and hence $\lim_{k \rightarrow \infty} z^{t_k+1} = z^*$.

Together with (12), (14) and (15), we have that

$$\begin{cases} \mathcal{C}^* &= \sum_{u=1}^3 \alpha_u \mathcal{X}_u^* *_u \mathcal{Y}_u^* + P_{\Omega} \left(\mathcal{M} - \sum_{u=1}^3 \alpha_u \mathcal{X}_u^* *_u \mathcal{Y}_u^* \right), \\ \hat{X}_u^{(l,*)} &= \alpha_u \bar{C}_u^{(l,*)} (Y^{(l,*)})^* \left(\alpha_u Y^{(l,*)} (Y^{(l,*)})^* + \lambda I \right)^{-1}, \quad u \in [\mathbf{3}], l \in [\mathbf{n}_u], \\ \hat{Y}_u^{(l,*)} &= \alpha_u \left(\alpha_u X^{(l,*)} (X^{(l,*)})^* + \lambda I \right)^{-1} \left(X_u^{(l,*)} \right)^* \bar{C}_u^{(l,*)}, \quad u \in [\mathbf{3}], l \in [\mathbf{n}_u]. \end{cases}$$

By direct computation, the following system is asserted

$$\begin{cases} \alpha_u(\hat{X}_u^* \hat{Y}_u^* - \bar{C}_u^*)(\hat{Y}^*)^* + \lambda \hat{X}^* = 0, & \forall u \in [\mathbf{3}] \\ \alpha_u(\hat{X}_u^*)^*(\hat{X}_u^* \hat{Y}_u^* - \bar{C}_u^*) + \lambda \hat{Y}_u^* = 0, & \forall u \in [\mathbf{3}] \\ P_\Omega(\mathcal{C}^* - \mathcal{M}) = 0, \\ P_{\Omega^c} \left(\sum_{u=1}^3 \alpha_u \mathcal{X}_u^* *_{*u} \mathcal{Y}_u^* - \mathcal{C}^* \right) = 0. \end{cases}$$

Therefore, z^* is a stationary point of problem (10).

(2). Since $\{z^t\}$ is bounded, there exists a compact convex set Z such that $\{z^t\} \subset Z$. Since f is a quadratic polynomial in z , the gradient ∇f is Lipschitz in Z with a Lipschitz constant L_f , that is,

$$\|\nabla f(z) - \nabla f(z')\|_F \leq L_f \|z - z'\|_F, \quad \forall z, z' \in Z.$$

Clearly,

$$\begin{aligned} & \left\| \prod_{\Omega} (\nabla_{\mathcal{C}} f(z^{t+1})) \right\|_F \\ & \leq \left\| \prod_{\Omega} (\nabla_{\mathcal{C}} f(\mathcal{C}^{t+1}, \mathcal{X}_1^{t+1}, \dots, \mathcal{Y}_3^{t+1})) - \prod_{\Omega} (\nabla_{\mathcal{C}} f(\mathcal{C}^t, \mathcal{X}_1^t, \dots, \mathcal{Y}_3^t)) \right\|_F \\ & \quad + \left\| \prod_{\Omega} (\nabla_{\mathcal{C}} f(\mathcal{C}^t, \mathcal{X}_1^t, \dots, \mathcal{Y}_3^t)) \right\|_F \\ & \leq L_f \|z^{t+1} - z^t\|_F + \left\| \left(\mathcal{C}^t - \sum_{u=1}^3 \alpha_u \mathcal{X}_u^t *_{*u} \mathcal{Y}_u^t \right) \right\|_{\Omega^c} \\ & = L_f \|z^{t+1} - z^t\|_F + \|\mathcal{C}^{t+1} - \mathcal{C}^t\|_F \\ & \leq (L_f + 1) \|z^{t+1} - z^t\|_F. \end{aligned}$$

Furthermore,

$$\begin{aligned} & \left\| \nabla_{\mathcal{X}_1} f(z^{t+1}) \right\|_F \\ & \leq \left\| \nabla_{\mathcal{X}_1} f(\mathcal{C}^{t+1}, \mathcal{X}_1^{t+1}, \dots, \mathcal{Y}_3^{t+1}) - \nabla_{\mathcal{X}_1} f(\mathcal{C}^{t+1}, \mathcal{X}_1^{t+1}, \dots, \mathcal{Y}_3^t) \right\|_F + \left\| \nabla_{\mathcal{X}_1} f(\mathcal{C}^{t+1}, \mathcal{X}_1^{t+1}, \dots, \mathcal{Y}_3^t) \right\|_F \\ & \leq L_f \|z^{t+1} - z^t\|_F + \lambda \|\mathcal{X}_u^{t+1} - \mathcal{X}_u^t\|_F \\ & \leq (L_f + \lambda) \|z^{t+1} - z^t\|_F. \end{aligned}$$

Similarly, for any $u \in [\mathbf{3}]$, we have

$$\begin{aligned} \left\| \nabla_{\mathcal{X}_u} f(z^{t+1}) \right\|_F & \leq (L_f + \lambda) \|z^{t+1} - z^t\|_F, \\ \left\| \nabla_{\mathcal{Y}_u} f(z^{t+1}) \right\|_F & \leq (L_f + \lambda) \|z^{t+1} - z^t\|_F. \end{aligned}$$

Now we can assert that $\left\| \prod_{\Omega} (\nabla f(z^{t+1})) \right\|_F \leq (7L_f + 6\lambda + 1) \|z^{t+1} - z^t\|_F$ and the result (2) is arrived with $\eta := 7L_f + 6\lambda + 1$. \blacksquare

Theorem 3.2 *Suppose that z^* is a limiting point of $\{z^t\}$ generated by MTRTC. Assume that the starting point z^0 satisfies $z^0 \in B(z^*, \sigma) := \{z : \|z - z^*\|_F < \sigma\} \subseteq Z'$, θ and μ are defined as in Definition 3.1. Suppose that $\rho = \frac{\min\{1, \lambda\}}{2\eta}$ with η and λ being from Theorem 3.1 (2) and*

$$\sigma > \frac{\mu}{\rho(1-\theta)} |f(z^0) - f(z^*)|^{1-\theta} + \|z^0 - z^*\|_F.$$

Then

(1). $z^t \in B(z^*, \sigma)$, for $t = 0, 1, 2, \dots$;

$$(2). \sum_{t=0}^{\infty} \|z^{t+1} - z^t\|_F \leq \frac{\mu}{\rho(1-\theta)} |f(z^0) - f(z^*)|^{1-\theta};$$

(3). The entire sequence $\{z^t\}$ converges.

Proof. We show (1) by induction. Clearly, (1) is true for $t = 0$ by assumption. Assume that (1) holds for all $t \leq \bar{t}$, then KL property holds for such $z^{\bar{t}}$. Now we show that (1) is true for $t = \bar{t} + 1$.

Let $\theta \in (0, 1)$ and $\phi(s) := \frac{\mu}{(1-\theta)} (s - f(z^*))^{1-\theta}$, $s \geq f(z^*)$. Then, $\phi(s)$ is concave with its derivative $\phi'(s) = \frac{\mu}{|s - f(z^*)|^\theta}$ for $s > f(z^*)$. Since $\phi(s)$ is concave, we have

$$\phi(f(z^t)) - \phi(f(z^{t+1})) \geq \phi'(f(z^t)) [f(z^t) - f(z^{t+1})] = \frac{\mu}{|f(z^t) - f(z^*)|^\theta} [f(z^t) - f(z^{t+1})].$$

Combining with (16) (17) and Theorem 3.1 (2), we have

$$\phi(f(z^t)) - \phi(f(z^{t+1})) \geq \frac{1}{\|\prod_{\Omega}(\nabla f(z^t))\|_F} [f(z^t) - f(z^{t+1})] \geq \rho \|z^{t+1} - z^t\|_F.$$

Hence,

$$\sum_{p=0}^t \|z^{k+1} - z^k\|_F \leq \frac{1}{\rho} \sum_{p=0}^t [\phi(f(z^t)) - \phi(f(z^{t+1}))] = \frac{1}{\rho} [\phi(f(z^0)) - \phi(f(z^{t+1}))] \leq \frac{1}{\rho} \phi(f(z^0)). \quad (18)$$

This implies that

$$\|z^{t+1} - z^*\|_F \leq \sum_{p=0}^t \|z_{t+1} - z_t\|_F + \|z^0 - z^*\|_F \leq \frac{1}{\rho} \phi(f(z^0)) + \|z^0 - z^*\|_F < \sigma.$$

Then we have $z^{t+1} \in B(z^*, \sigma)$, and hence (1) is asserted.

(2). Taking $t \rightarrow \infty$ in (18), (2) is arrived.

(3). From (2), for any $\epsilon > 0$, there exists $K_1 > 0$ such that for any $t \geq K_1$ such that $\|z^t - z^{t_k}\|_F \leq \sum_{i=1}^{t_k-t} \|z^{t+i} - z^{t+i-1}\|_F < \frac{\epsilon}{2}$. From $\lim_{k \rightarrow \infty} z^{t_k} = z^*$, there exists $K_2 > 0$ such that for all $k > K_2$, $\|z^{t_k} - z^*\|_F < \frac{\epsilon}{2}$. Hence, for any $t \geq \max\{K_1, K_2\}$,

$$\|z^t - z^*\|_F \leq \|z^t - z^{t_k}\|_F + \|z^{t_k} - z^*\|_F \leq \epsilon,$$

which indicates that $z^t \rightarrow z^*$. ■

Theorem 3.3 Suppose that $\{z^t\}$ is an infinite sequence generated by MTRTC with an accumulating point z^* and θ, μ are as in Definition 3.1. Then

(a). If $\theta \in (0, \frac{1}{2}]$, then there exist $\gamma > 0$ and $c \in (0, 1)$ such that

$$\|z^t - z^*\|_F \leq \gamma c^t;$$

(b). If $\theta \in (\frac{1}{2}, 1)$, then there exists $\gamma > 0$ such that

$$\|z^t - z^*\|_F \leq \gamma t^{-\frac{1-\theta}{2\theta-1}}.$$

Proof. Assume that $z^0 \in B(z^*, \sigma)$. Denote that

$$\Delta_t := \sum_{p=t}^{\infty} \|z^p - z^{p+1}\|_F.$$

Then

$$\|z^t - z^*\|_F \leq \Delta_t. \quad (19)$$

From Theorem 3.2 (2), we have

$$\Delta_t \leq \frac{\mu}{\rho(1-\theta)} |f(z^0) - f(z^*)|^{1-\theta} = \frac{\mu}{\rho(1-\theta)} \left[|f(z^0) - f(z^*)|^\theta \right]^{\frac{1-\theta}{\theta}}.$$

Combining with the KL inequality, there holds

$$\Delta_t \leq \frac{\mu}{\rho(1-\theta)} \left(\mu \left\| \prod_{\Omega} (\nabla f(z)) \right\|_F \right)^{\frac{1-\theta}{\theta}}.$$

From Theorem 3.1 (2), the above inequality implies that

$$\Delta_t \leq \frac{\mu}{\rho(1-\theta)} (\mu\eta \|z^t - z^{t+1}\|_F)^{\frac{1-\theta}{\theta}} = c_1 (\Delta_t - \Delta_{t+1})^{\frac{1-\theta}{\theta}}. \quad (20)$$

where $c_1 = \frac{\mu}{\rho(1-\theta)} (\mu\eta)^{\frac{1-\theta}{\theta}}$ is a positive constant.

(a). If $\theta \in (0, \frac{1}{2}]$, then $\frac{1-\theta}{\theta} \geq 1$. For sufficiently large t , it holds

$$\Delta_t \leq c_1 (\Delta_t - \Delta_{t+1}).$$

Hence

$$\Delta_{t+1} \leq \frac{c_1 - 1}{c_1} \Delta_t.$$

Together with (19), result (a) is arrived with $c = \frac{c_1 - 1}{c_1}$.

(b). For case of $\theta \in (\frac{1}{2}, 1)$, let $h(s) = s^{-\frac{\theta}{1-\theta}}$. The function $h(s)$ is monotonically decreasing on s . By (20), we have

$$c_1^{-\frac{\theta}{1-\theta}} \leq h(\Delta_t) (\Delta_t - \Delta_{t+1}) = \int_{\Delta_{t+1}}^{\Delta_t} h(s) ds \leq \int_{\Delta_{t+1}}^{\Delta_t} h(s) ds = -\frac{1-\theta}{2\theta-1} \left(\Delta_t^{-\frac{2\theta-1}{1-\theta}} - \Delta_{t+1}^{-\frac{2\theta-1}{1-\theta}} \right).$$

Since $\theta \in (\frac{1}{2}, 1)$, $\nu := -\frac{2\theta-1}{1-\theta} < 0$ and $\Delta_{t+1}^\nu - \Delta_t^\nu \geq -\nu c_1^{-\frac{\theta}{1-\theta}} > 0$. Thus, there is a \hat{t} such that for all $t \geq 2\hat{t}$,

$$\Delta_t^\nu \geq \Delta_{\hat{t}}^\nu - \nu c_1^{-\frac{\theta}{1-\theta}} (t - \hat{t}) \geq -\nu c_1^{-\frac{\theta}{1-\theta}} (t - \hat{t}) \geq -\frac{\nu}{2} c_1^{-\frac{\theta}{1-\theta}} t,$$

then we have

$$\Delta_t \leq \gamma t^{\frac{1}{\nu}},$$

for a certain positive constant $\gamma = \left(-\frac{\nu}{2} c_1^{-\frac{\theta}{1-\theta}} \right)^{\frac{1}{\nu}}$. Then result (b) is obtained. \blacksquare

4 Improvement with spatio-temporal characteristics

In practical applications, some characteristics are included. For example, both the video data between two adjacent frames and the internet traffic data of two adjacent days are temporal stability features. To characterize such properties, some constraint matrices are considered.

As in [31, 41], the temporal constraint matrix H captures the temporal stability feature, i.e., the data is similar at adjacent time slots in the tensor. Let $H = \text{Toeplitz}(0, 1, -1)$ be a Toeplitz matrix of size $(n_3 - 1) \times n_3$ with

$$H = \begin{bmatrix} 1 & -1 & 0 & \cdots \\ 0 & 1 & -1 & \ddots \\ 0 & 0 & 1 & \ddots \\ \vdots & \ddots & \ddots & \ddots \end{bmatrix}_{(n_3-1) \times n_3}.$$

Let n_3 be the time dimension. Then the time stability is expressed by minimizing

$$\|\mathcal{C} \times_3 H\|_F^2 = \sum_{k=1}^{n_3-1} \left\| \mathcal{C}_3^{(k)} - \mathcal{C}_3^{(k+1)} \right\|_F^2.$$

Let the spatial constraint matrices F and G capture spatial correlation feature. We choose F and G according to the similarity between $\mathcal{C}_1^{(i)}$ and $\mathcal{C}_1^{(j)}$ ($j \neq i$), $\mathcal{C}_2^{(i)}$ and $\mathcal{C}_2^{(j)}$ ($j \neq i$), respectively. For each $\mathcal{C}_1^{(i)}$, we perform linear regression to find a set of weights $w_i(j)$ such that the linear combination of $\mathcal{C}_1^{(j)}$ is a best approximation of $\mathcal{C}_1^{(i)}$, i.e., $\mathcal{C}_1^{(i)} = \sum_{j \neq i} w_i(j) \mathcal{C}_1^{(j)}$. Then we set $F(i, i) = 1$ and $F(i, j) = -w_i(j)$. Matrix G can be obtained similarly. Let n_1 and n_2 be the spatial dimensions. Then the spatial correlation features can be expressed by minimizing

$$\|\mathcal{C} \times_1 F\|_F^2 = \sum_{i=1}^{n_1} \left\| \mathcal{C}_1^{(i)} - \sum_{j \neq i} w_i(j) \mathcal{C}_1^{(j)} \right\|_F^2$$

and

$$\|\mathcal{C} \times_2 G\|_F^2 = \sum_{i=1}^{n_2} \left\| \mathcal{C}_2^{(i)} - \sum_{j \neq i} w_i(j) \mathcal{C}_2^{(j)} \right\|_F^2.$$

Before we get such matrices F and G , it is necessary to estimate an initial tensor \mathcal{C} without missing data and outlier because these factors may destroy spatial features. To this end, we first recover the missing entries and remove outlier by using the temporal constraint (i.e., H). For the estimated tensor \mathcal{C} , we analyze the similarities and linear regression to find spatial constraints (i.e., F, G). Then the obtained F, G are used together with matrix H in algorithm to recovery the data.

Based on the three matrices F, G and H , the tensor factorization model (10) can be modified as

$$\begin{aligned} \min_{\mathcal{X}_u, \mathcal{Y}_u, \mathcal{C}} \quad & \sum_{u=1}^3 \frac{\alpha_u}{2} \|\mathcal{X}_u * \mathcal{Y}_u - \mathcal{C}\|_F^2 + \frac{\beta_1}{2} \|(\mathcal{X}_2 * \mathcal{Y}_2) \times_1 F\|_F^2 \\ & + \frac{\beta_2}{2} \|(\mathcal{X}_3 * \mathcal{Y}_3) \times_2 G\|_F^2 + \frac{\beta_3}{2} \|(\mathcal{X}_1 * \mathcal{Y}_1) \times_3 H\|_F^2 \\ \text{s.t.} \quad & P_\Omega(\mathcal{C} - \mathcal{M}) = 0. \end{aligned} \tag{21}$$

Let $\beta_u = 0$ if there is no additional characteristics on the u th dimension of data. Hence, model (13) can be regarded as a special case of model (21).

With Lemma 2.2, (21) can be rewritten as

$$\begin{aligned} \min_{\mathcal{X}_u, \mathcal{Y}_u, \mathcal{C}} \quad & \sum_{u=1}^3 \frac{\alpha_u}{2} \|\mathcal{X}_u * \mathcal{Y}_u - \mathcal{C}\|_F^2 + \frac{\beta_1}{2} \|\mathcal{F} *_2 (\mathcal{X}_2 *_2 \mathcal{Y}_2)\|_F^2 \\ & + \frac{\beta_2}{2} \|(\mathcal{X}_3 *_3 \mathcal{Y}_3) *_3 \mathcal{G}\|_F^2 + \frac{\beta_3}{2} \|(\mathcal{X}_1 *_1 \mathcal{Y}_1) *_1 \mathcal{H}\|_F^2 \\ \text{s.t.} \quad & P_\Omega(\mathcal{C} - \mathcal{M}) = 0. \end{aligned} \quad (22)$$

Similar to solve (8), we consider the regularized version of problem (22), which can be written as

$$\min_{\mathcal{C}, \mathcal{X}_u, \mathcal{Y}_u} g(\mathcal{C}, \mathcal{X}_1, \mathcal{X}_2, \mathcal{X}_3, \mathcal{Y}_1, \mathcal{Y}_2, \mathcal{Y}_3), \quad \text{s.t.} \quad P_\Omega(\mathcal{C} - \mathcal{M}) = 0, \quad (23)$$

where

$$\begin{aligned} & g(\mathcal{C}, \mathcal{X}_1, \mathcal{X}_2, \mathcal{X}_3, \mathcal{Y}_1, \mathcal{Y}_2, \mathcal{Y}_3) \\ &= \sum_{u=1}^3 \frac{\alpha_u}{2} \|\mathcal{X}_u * \mathcal{Y}_u - \mathcal{C}\|_F^2 + \frac{\beta_1}{2} \|\mathcal{F} *_2 (\mathcal{X}_2 *_2 \mathcal{Y}_2)\|_F^2 + \frac{\beta_2}{2} \|(\mathcal{X}_3 *_3 \mathcal{Y}_3) *_3 \mathcal{G}\|_F^2 + \frac{\beta_3}{2} \|(\mathcal{X}_1 *_1 \mathcal{Y}_1) *_1 \mathcal{H}\|_F^2 \\ &+ \frac{\lambda}{2} (2\beta_1 \|\mathcal{F} *_2 \mathcal{X}_2\|_F^2 + \alpha_2 \|\mathcal{X}_2\|_F^2 + \|\mathcal{Y}_2\|_F^2) + \frac{\lambda}{2} (\|\mathcal{X}_3\|_F^2 + 2\beta_2 \|\mathcal{Y}_3 *_3 \mathcal{G}\|_F^2 + \alpha_3 \|\mathcal{Y}_3\|_F^2) \\ &+ \frac{\lambda}{2} (\|\mathcal{X}_1\|_F^2 + 2\beta_3 \|\mathcal{Y}_1 *_1 \mathcal{H}\|_F^2 + \alpha_1 \|\mathcal{Y}_1\|_F^2). \end{aligned}$$

Clearly, \mathcal{C}^{t+1} can be updated by (12). Hence it suffices to consider how to update \mathcal{X}_u^{t+1} and \mathcal{Y}_u^{t+1} for all $u \in [3]$. From the structure of \hat{X}_u and \hat{Y}_u in section 2, we have

$$\begin{aligned} \|\mathcal{F} *_2 (\mathcal{X}_2 *_2 \mathcal{Y}_2)\|_F^2 &= \frac{1}{n_2} \|\bar{F}_2(\overline{\mathcal{X}_2 *_2 \mathcal{Y}_2})\|_F^2 = \frac{1}{n_2} \|\bar{F}_2(\bar{X}_2 \bar{Y}_2)\|_F^2 \\ &= \frac{1}{n_2} \|\bar{F}_2(\hat{X}_2 \hat{Y}_2)\|_F^2 = \frac{1}{n_2} \|\bar{F}_2 \hat{X}_2 \hat{Y}_2\|_F^2 = \frac{1}{n_2} \sum_{j=1}^{n_2} \|\bar{F}_2^{(j)} \hat{X}_2^{(j)} \hat{Y}_2^{(j)}\|_F^2. \end{aligned}$$

Similarly, we have

$$\|(\mathcal{X}_3 *_3 \mathcal{Y}_3) *_3 \mathcal{G}\|_F^2 = \frac{1}{n_3} \sum_{k=1}^{n_3} \|\hat{X}_3^{(k)} \hat{Y}_3^{(k)} \bar{G}_3^{(k)}\|_F^2, \quad \|(\mathcal{X}_1 *_1 \mathcal{Y}_1) *_1 \mathcal{H}\|_F^2 = \frac{1}{n_1} \sum_{i=1}^{n_1} \|\hat{X}_1^{(i)} \hat{Y}_1^{(i)} \bar{H}_1^{(i)}\|_F^2.$$

Based on these results, we can rewrite (23) as the following matrix version

$$\begin{aligned} \min_{\mathcal{C}, \hat{X}_u, \hat{Y}_u} \quad & \sum_{l=1}^{n_u} \frac{\alpha_u}{2n_u} \|\hat{X}_u^{(l)} \hat{Y}_u^{(l)} - \bar{C}_u^{(l)}\|_F^2 + \frac{\beta_1}{2n_2} \sum_{j=1}^{n_2} \|\bar{F}_2^{(j)} \hat{X}_2^{(j)} \hat{Y}_2^{(j)}\|_F^2 \\ & + \frac{\beta_2}{2n_3} \sum_{k=1}^{n_3} \|\hat{X}_3^{(k)} \hat{Y}_3^{(k)} \bar{G}_3^{(k)}\|_F^2 + \frac{\beta_3}{2n_1} \sum_{i=1}^{n_1} \|\hat{X}_1^{(i)} \hat{Y}_1^{(i)} \bar{H}_1^{(i)}\|_F^2 \\ & + \lambda \left(\frac{\beta_1}{n_2} \sum_{j=1}^{n_2} \|\bar{F}_2^{(j)} \hat{X}_2^{(j)}\|_F^2 + \frac{\alpha_2}{2n_2} \sum_{j=1}^{n_2} \|\hat{X}_2^{(j)}\|_F^2 + \frac{1}{2n_2} \sum_{j=1}^{n_2} \|\hat{Y}_2^{(j)}\|_F^2 \right) \\ & + \lambda \left(\frac{1}{2n_3} \sum_{k=1}^{n_3} \|\hat{X}_3^{(k)}\|_F^2 + \frac{\beta_2}{n_3} \sum_{k=1}^{n_3} \|\hat{Y}_3^{(k)} \bar{G}_3^{(k)}\|_F^2 + \frac{\alpha_3}{2n_3} \sum_{k=1}^{n_3} \|\hat{Y}_3^{(k)}\|_F^2 \right) \\ & + \lambda \left(\frac{1}{2n_1} \sum_{i=1}^{n_1} \|\hat{X}_1^{(i)}\|_F^2 + \frac{\beta_3}{n_1} \sum_{i=1}^{n_1} \|\hat{Y}_1^{(i)} \bar{H}_1^{(i)}\|_F^2 + \frac{\alpha_1}{2n_1} \sum_{i=1}^{n_1} \|\hat{Y}_1^{(i)}\|_F^2 \right). \end{aligned}$$

To update \mathcal{X}_1^{t+1} and \mathcal{Y}_1^{t+1} , we consider the following problem

$$\begin{aligned} & \min_{\hat{X}_1, \hat{Y}_1} \sum_{i=1}^{n_1} \frac{\alpha_1}{2n_1} \left\| \hat{X}_1^{(i)} \hat{Y}_1^{(i)} - \bar{C}_1^{(i)} \right\|_F^2 + \frac{\beta_3}{2n_1} \sum_{i=1}^{n_1} \left\| \hat{X}_1^{(i)} \hat{Y}_1^{(i)} \bar{H}_1^{(i)} \right\|_F^2 \\ & + \lambda \left(\frac{1}{2n_1} \sum_{i=1}^{n_1} \left\| \hat{X}_1^{(i)} \right\|_F^2 + \frac{\beta_3}{n_1} \sum_{i=1}^{n_1} \left\| \hat{Y}_1^{(i)} \bar{H}_1^{(i)} \right\|_F^2 + \frac{\alpha_1}{2n_1} \sum_{i=1}^{n_1} \left\| \hat{Y}_1^{(i)} \right\|_F^2 \right). \end{aligned}$$

For any $i \in [\mathbf{n}_1]$, $\hat{X}_1^{(i,t+1)}$ and $\hat{Y}_1^{(i,t+1)}$ are updated by

$$\begin{aligned} \hat{X}_1^{(i,t+1)} = & \left(\lambda \hat{X}_1^{(i,t)} + \alpha_1 \bar{C}_1^{(i,t+1)} \left(\hat{Y}_1^{(i,t)} \right)^* \right) \left[\alpha_1 \hat{Y}_1^{(i,t)} \left(\hat{Y}_1^{(i,t)} \right)^* + \right. \\ & \left. \beta_3 \left(\hat{Y}_1^{(i,t)} \bar{H}_1^{(i)} \right) \left(\hat{Y}_1^{(i,t)} \bar{H}_1^{(i)} \right)^* + 2\lambda I \right]^{-1} \end{aligned} \quad (24)$$

and

$$\begin{aligned} \hat{Y}_1^{(i,t+1)} = & \alpha_1 \left[\left(\hat{X}_1^{(i,t+1)} \right)^* \hat{X}_1^{(i,t+1)} + 2\lambda I \right]^{-1} \left(\lambda \hat{Y}_1^{(i,t)} + \left(\hat{X}_1^{(i,t+1)} \right)^* \bar{C}_1^{(i,t+1)} \right) \\ & \left[\alpha_1 I + \beta_3 \bar{H}_1^{(i)} \left(\bar{H}_1^{(i)} \right)^* \right]^{-1}. \end{aligned} \quad (25)$$

To update \mathcal{X}_2^{t+1} and \mathcal{Y}_2^{t+1} , we consider the following problem

$$\begin{aligned} & \min_{\hat{X}_2, \hat{Y}_2} \sum_{j=1}^{n_2} \frac{\alpha_2}{2n_2} \left\| \hat{X}_2^{(j)} \hat{Y}_2^{(j)} - \bar{C}_2^{(j)} \right\|_F^2 + \frac{\beta_1}{2n_2} \sum_{j=1}^{n_2} \left\| \bar{F}_2^{(j)} \hat{X}_2^{(j)} \hat{Y}_2^{(j)} \right\|_F^2 \\ & + \lambda \left(\frac{\beta_1}{n_2} \sum_{j=1}^{n_2} \left\| \bar{F}_2^{(j)} \hat{X}_2^{(j)} \right\|_F^2 + \frac{\alpha_2}{2n_2} \sum_{j=1}^{n_2} \left\| \hat{X}_2^{(j)} \right\|_F^2 + \frac{1}{2n_2} \sum_{j=1}^{n_2} \left\| \hat{Y}_2^{(j)} \right\|_F^2 \right). \end{aligned}$$

Therefore, for any $j \in [\mathbf{n}_2]$, $\hat{X}_2^{(j,t+1)}$ and $\hat{Y}_2^{(j,t+1)}$ are updated by

$$\begin{aligned} \hat{X}_2^{(j,t+1)} = & \alpha_2 \left[\alpha_2 I + \beta_1 \left(\bar{F}_2^{(j)} \right)^* \bar{F}_2^{(j)} \right]^{-1} \left(\lambda \hat{X}_2^{(j,t)} + \bar{C}_2^{(j,t+1)} \left(\hat{Y}_2^{(j,t)} \right)^* \right) \\ & \left[\hat{Y}_2^{(j,t)} \left(\hat{Y}_2^{(j,t)} \right)^* + 2\lambda I \right]^{-1} \end{aligned} \quad (26)$$

and

$$\begin{aligned} \hat{Y}_2^{(j,t+1)} = & \left[\alpha_2 \left(\hat{X}_2^{(j,t+1)} \right)^* \hat{X}_2^{(j,t+1)} + \beta_1 \left(\bar{F}_2^{(j)} \hat{X}_2^{(j,t+1)} \right)^* \bar{F}_2^{(j)} \hat{X}_2^{(j,t+1)} + 2\lambda I \right]^{-1} \\ & \left(\lambda \hat{Y}_2^{(j,t)} + \alpha_2 \left(\hat{X}_2^{(j,t+1)} \right)^* \bar{C}_2^{(j,t+1)} \right). \end{aligned} \quad (27)$$

To update \mathcal{X}_3^{t+1} and \mathcal{Y}_3^{t+1} , we consider the following problem

$$\begin{aligned} & \min_{\hat{X}_3, \hat{Y}_3} \sum_{k=1}^{n_3} \frac{\alpha_3}{2n_3} \left\| \hat{X}_3^{(k)} \hat{Y}_3^{(k)} - \bar{C}_3^{(k)} \right\|_F^2 + \frac{\beta_2}{2n_3} \sum_{k=1}^{n_3} \left\| \hat{X}_3^{(k)} \hat{Y}_3^{(k)} \bar{G}_3^{(k)} \right\|_F^2 \\ & + \lambda \left(\frac{1}{2n_3} \sum_{k=1}^{n_3} \left\| \hat{X}_3^{(k)} \right\|_F^2 + \frac{\beta_2}{n_3} \sum_{k=1}^{n_3} \left\| \hat{Y}_3^{(k)} \bar{G}_3^{(k)} \right\|_F^2 + \frac{\alpha_3}{2n_3} \sum_{k=1}^{n_3} \left\| \hat{Y}_3^{(k)} \right\|_F^2 \right). \end{aligned}$$

Then $\hat{X}_3^{(k,t+1)}$ and $\hat{Y}_3^{(k,t+1)}$ for any $k \in [\mathbf{n}_3]$ are updated by

$$\begin{aligned} \hat{X}_3^{(k,t+1)} = & \left(\lambda \hat{X}_3^{(k,t)} + \alpha_3 \bar{C}_3^{(k,t+1)} \left(\hat{Y}_3^{(k,t)} \right)^* \right) \left[\alpha_3 \hat{Y}_3^{(k,t)} \left(\hat{Y}_3^{(k,t)} \right)^* + \right. \\ & \left. \beta_2 \left(\hat{Y}_3^{(k,t)} \bar{G}_3^{(k)} \right) \left(\hat{Y}_3^{(k,t)} \bar{G}_3^{(k)} \right)^* + 2\lambda I \right]^{-1} \end{aligned} \quad (28)$$

and

$$\hat{Y}_3^{(k,t+1)} = \alpha_3 \left[\left(\hat{X}_3^{(k,t+1)} \right)^* \hat{X}_3^{(k,t+1)} + 2\lambda I \right]^{-1} \left(\lambda \hat{Y}_3^{(k,t)} + \left(\hat{X}_3^{(k,t+1)} \right)^* \bar{C}_3^{(k,t+1)} \right). \quad (29)$$

$$\left[\alpha_3 I + \beta_2 \bar{G}_3^{(k)} \left(\bar{G}_3^{(k)} \right)^* \right]^{-1}.$$

Based on above analysis, the alternating minimization method can be outlined as Algorithm 4.1, denoted by ST-MTRTC for convenience.

Algorithm 4.1 Spatio-Temporal Multi-Tubal Rank Tensor Completion (ST-MTRTC)

Input: The tensor data $\mathcal{M} \in \mathbb{C}^{n_1 \times n_2 \times n_3}$, $\mathcal{H} \in \mathbb{R}^{n_1 \times n_3 \times n_3}$, the observed set Ω , the initialized rank R^0 , parameters λ , ε and α_u , $u \in [\mathbf{3}]$.

Initialization: \hat{X}_u^0, \hat{Y}_u^0 , $u \in [\mathbf{3}]$.

While not converge do

1. Fix \hat{X}_u^t and \hat{Y}_u^t , compute \mathcal{C}^{t+1} by (12).
2. Compute \mathcal{F} and \mathcal{G} based on \mathcal{C}^1 .
3. Compute \hat{X}_u^{t+1} by (24),(26) and (28) by fixing \hat{Y}_u^t and \mathcal{C}^{t+1} .
4. Obtain \hat{Y}_u^{t+1} by (25),(27) and (29) based on \hat{X}_u^{t+1} and \mathcal{C}^{t+1} .
5. Adopt the rank decreasing scheme to adjust $rank_{mt}(\mathcal{A})$ and the sizes of \hat{X}_u^{t+1} and \hat{Y}_u^{t+1} .
6. Check the stop criterion $\|\mathcal{C}_\Omega^{t+1} - \mathcal{M}_\Omega\|_F / \|\mathcal{M}_\Omega\|_F < \varepsilon$.
7. $t \leftarrow t + 1$.

end while

Output: \mathcal{C}^{t+1} .

The convergence is similar to that of Algorithm MTRTC and hence we omit it here.

5 Numerical Experiments

In this section, we report some numerical results of our proposed algorithms MTRTC and ST-MTRTC to show the validity. We adopt the relative error and the peak signal-to-noise ratio (PSNR) as evaluation metrics, which are defined by

$$\text{RSE} := \frac{\|\hat{\mathcal{C}} - \mathcal{M}\|_F}{\|\mathcal{M}\|_F}, \quad \text{PSNR} := 10 \log_{10} \left(\frac{n_1 n_2 n_3 \|\mathcal{M}\|_\infty^2}{\|\hat{\mathcal{C}} - \mathcal{M}\|_F^2} \right),$$

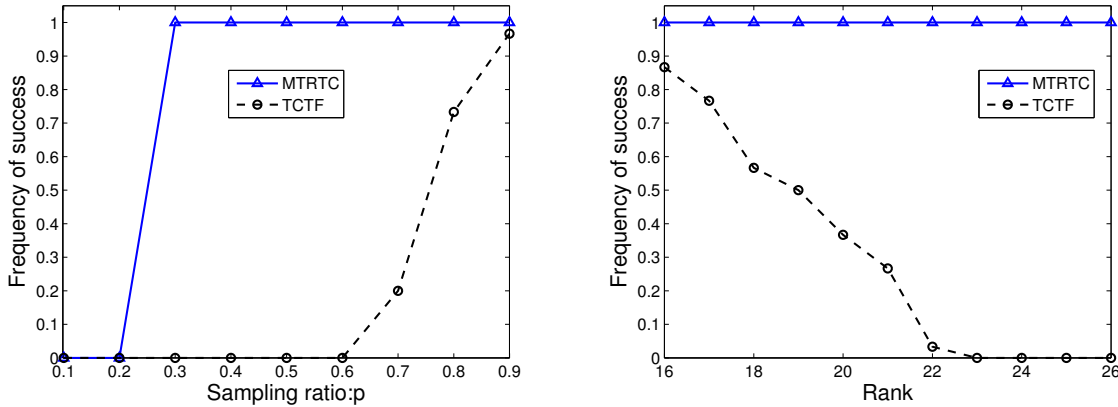
where \mathcal{M} and $\hat{\mathcal{C}}$ are the observed tensor and estimated tensor, respectively. The parameter λ is set as 0.1 in both MTRTC and ST-MTRTC. We conduct extensive experiments to evaluate our methods, and then compare the results with those by some other existing methods, including TMac [38] and TCTF [42]. All the methods are implemented on the platform of Windows 10 and Matlab (R2014a) with an Intel(R) Core(TM) i7-7700 CPU at 3.60GHz and 8 GB RAM.

5.1 Numerical Simulation

In this subsection, we test MTRTC on synthetic data to evaluate the efficiency by comparing MTRTC with TCTF. In experiments, the maximum iteration number is set to be 300 and the termination precision ε is set to be $1e-5$.

The tested tensor $\mathcal{M} \in \mathbb{R}^{100 \times 100 \times 100}$ is constructed in the following way. Use Matlab command `randn(r1,r2,r3)` to generate tensor $\mathcal{B} \in \mathbb{R}^{r_1 \times r_2 \times r_3}$. Generate matrices $U^i \in \mathbb{R}^{100 \times r_i}$ with $i \in [3]$ such that the multi-rank of tensor $\mathcal{M} := \mathcal{B} \times_1 U^1 \times_2 U^2 \times_3 U^3$ is (r_1, r_2, r_3) . Select $pn_1n_2n_3$ positions of \mathcal{M} uniformly to construct Ω , where p is the sampling ratio. If $RSE < 1e-3$, $\hat{\mathcal{C}}$ is regarded as a successful recovery to \mathcal{M} . For fairness, we run these procedures for 30 times.

First, we test TCTF and MTRTC for the problems of different sample rates. Let $r_1 = r_2 = r_3 = 20$, the initial rank $(r_u^l)^0 = 20$, $u \in [3]$, $l \in [\mathbf{n}_u]$ in MTRTC and the initial rank $(20, 20, 20)$ in TCTF. We set sampling ratio p varying from 0.1 to 0.9 with increment 0.1. The numerical results are reported in Figure 2 (a).



(a) Comparison on frequency of success of different sampling ratios (b) Comparison on frequency of success of different ranks

Figure 2: Comparison on frequency of success obtained by MTRTC and TCTF

In Figure 2 (a), the frequency of success of these two methods are reported. Our proposed method MTRTC performs much better than TCTF. We find that the lower the sampling ratio p , the more difficult it is to recover the tensor successfully. From Figure 2 (a), it is clear that our method MTRTC can complete the tensor successfully when the sample rate is bigger than 0.2; while the tensor can not be completed by TCTF when the sample rate is less than 0.6.

On the other hand, we test TCTF and MTRTC for the tested tensors of sampling ratio $p = 0.7$ with different ranks. We set the rank $r = r_1 = r_2 = r_3$ varying from 16 to 26 with increment 1. We set the initialized rank $(r_u^l)^0 = r$, $u \in [3]$, $l \in [\mathbf{n}_u]$ in MTRTC and the initial rank (r, r, r) in TCTF. The frequencies of success are reported in Figure 2 (b).

Figure 2 (b) indicates that tensor can be completed by MTRTC for all estimated rank from $(16, 16, 16)$. With the increase of rank, the success rate of TCTF in restoring tensors gradually decreases. Moreover,

Table 1: Comparison of the PSNR, the RSE and the running time by MTRTC, TCTF and TMac

Image \ Method	MTRTC			TCTF			TMac		
	PSNR	RSE	time	PSNR	RSE	time	PSNR	RSE	time
Flower	32.07	0.079	9.51	30.95	0.090	13.28	24.09	0.199	11.47
Desert	36.61	0.031	9.02	30.72	0.060	12.08	28.96	0.074	12.00
River otter	34.95	0.052	9.23	29.08	0.102	11.89	26.95	0.131	11.67
Viaduct	37.23	0.031	9.11	32.63	0.053	11.69	27.74	0.093	11.24
House	33.88	0.038	9.26	28.91	0.067	12.11	26.89	0.084	11.48
Man	30.41	0.056	9.00	26.15	0.092	12.03	23.37	0.127	11.70
Human	29.80	0.064	10.41	27.97	0.079	11.91	23.84	0.127	11.31
Girl	32.92	0.049	9.88	26.49	0.103	12.99	25.12	0.121	11.46
Average	34.60	0.043	9.65	29.59	0.079	11.46	27.31	0.101	11.09

TCTF cannot successfully restore tensors when the rank is bigger than 22.

From accuracy and efficiency, we know that MTRTC performs better than TCTF for all sizes of the sampling ratios and tensor ranks.

5.2 Image Simulation

In this subsection, we apply MTRTC to color image inpainting. Note that color images can be expressed as third order tensors. When the tensor data is of low rank, or numerical low rank, the image inpainting problem can be modeled as a tensor completion problem. We use the Berkeley Segmentation database [27] to evaluate our method for image inpainting. It has a total of 200 color images, of size $321 \times 481 \times 3$. In these experiments, we compare our results with those from the state-of-the-art methods (TMac, TCTF).

In the test, all 200 images are chosen from the Berkeley Segmentation database. For each chosen image, we randomly sample by sampling ratio $p = 0.7$. We set the initial multi-tubal rank $(r_u^l)^0 = 2, u \in [2], (r_3^l)^0 = 30, l \in [\mathbf{n}_u]$ in MTRTC, the initial tubal rank $(30, 30, 30)$ in TCTF and the initial Tucker rank $(30, 30, 3)$ in TMac. In experiments, the maximum iteration number is set to be 300 and the termination precision ϵ is set to be $1e-5$.

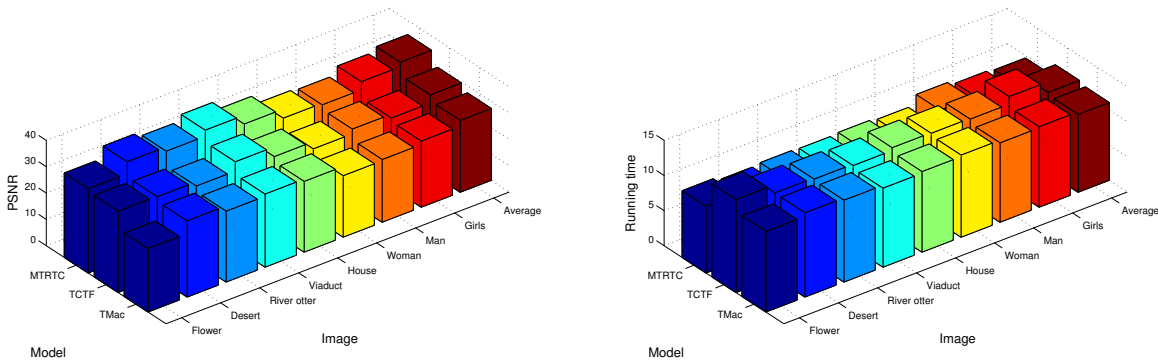
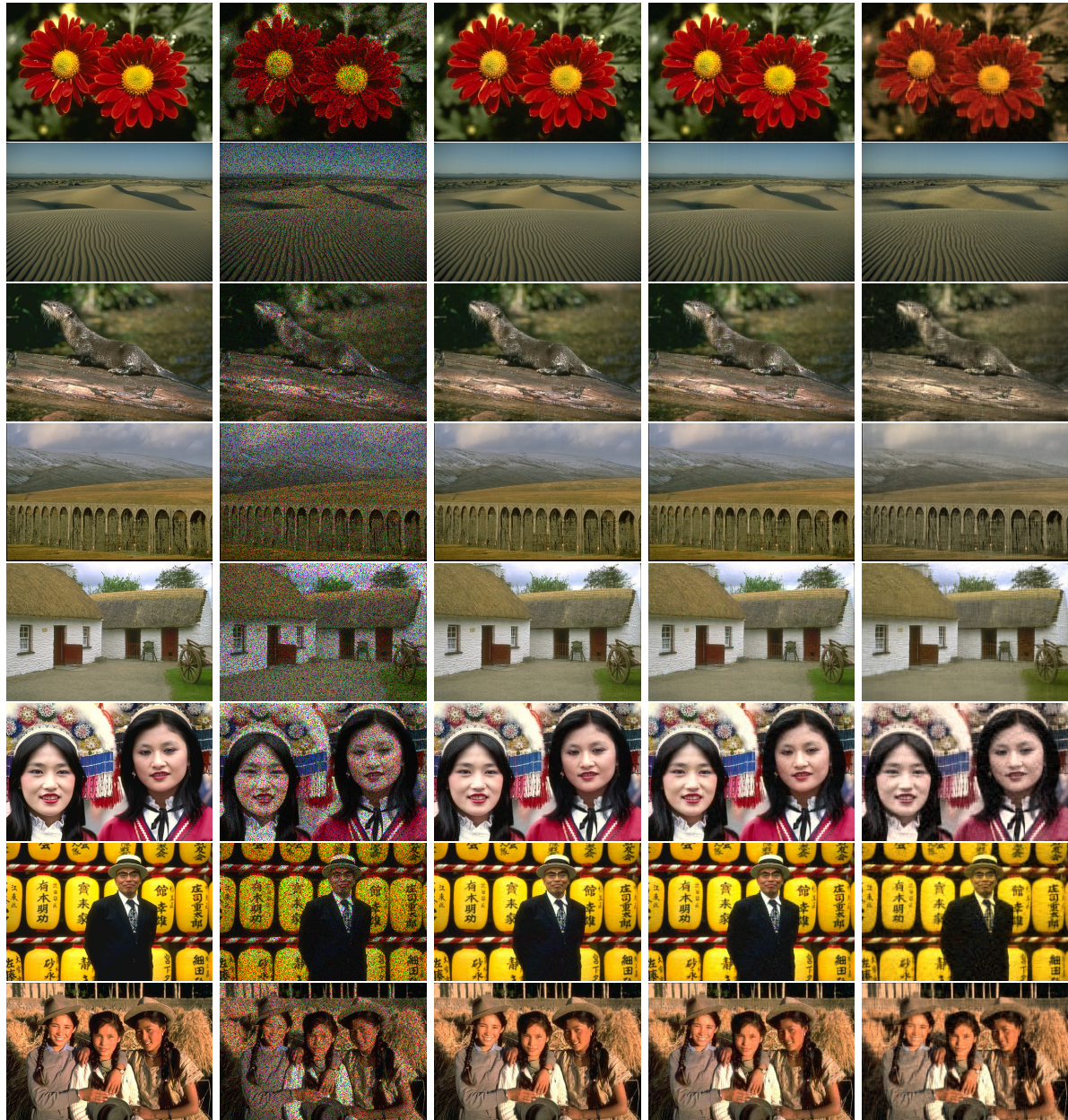


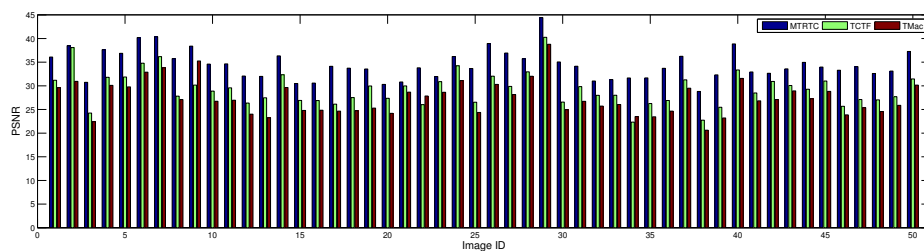
Figure 3: Comparison on the PSNR and the running time by MTRTC, TCTF and TMac



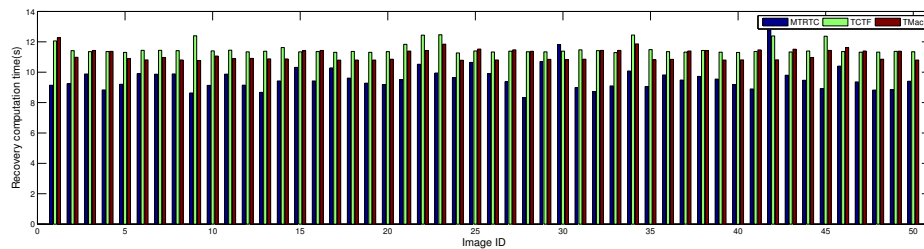
(a) Original (b) Observation (c) MTRTC (d) TCTF (e) TMac

Figure 4: Recovery performance comparison on the 8 images by MTRTC, TCTF and TMac

We present the image inpainting results of the eight tested images in Table 1, Figure 3 and Figure 4, in which “Average” denotes the average inpainting results of all 200 images. “Average” indicates that MTRTC outperforms TCTF and TMac. As stated in [15, 40], TMac expands the tensor data directly into matrices and applies matrix nuclear norm to approximate matrix rank, which may destroy multi-data structures and cause performance degradation. Based on tensor factorization, TCTF and MTRTC avoid the loss of tensor structure information [15, 40], thus obtain better inpainting results. Although TCTF requires less time in each iteration, it takes more iterations to converge, see the running time in Table 1. Furthermore, MTRTC takes account of all the modes, which is more comprehensive to preserve all low rank structure of tensor data. From Figure 3, MTRTC is the fastest one, which needs about 2/3 times running time of TCTF and TMac.



(a) Comparison of the PSNR values on 50 images



(b) Comparison of the running time on 50 images

Figure 5: Comparison of the PSNR and the running time on 50 images

In Figure 5, we report the PSNR values and the running time of all methods on the first 50 images. MTRTC performs the best with at least 1.2 times improvement upon the PSNR metric on all 50 images, verifying its advantages and robustness. From Figure 5 (b), MTRTC is much faster than other compared methods. In conclusion, it not only achieves the best inpainting results but also runs within least running time.

For further comparison, we also recover images of the deterministically masked images by grids, leaves and letters, respectively. In experiments, the maximum iteration number is set to be 500 and the termination precision ε is set to be $1e-5$. Clearly, the masked images are no-mean-sampling. The results are displayed in Figure 6 and Table 2, which show that TCTF and MTRTC have better performance than TMac. Furthermore, the effect of MTRTC is much better than that of TCTF. Table 2 reports all numerical results of three methods. We can assert that MTRTC is the best one in MTRTC, TCTF and TMac.

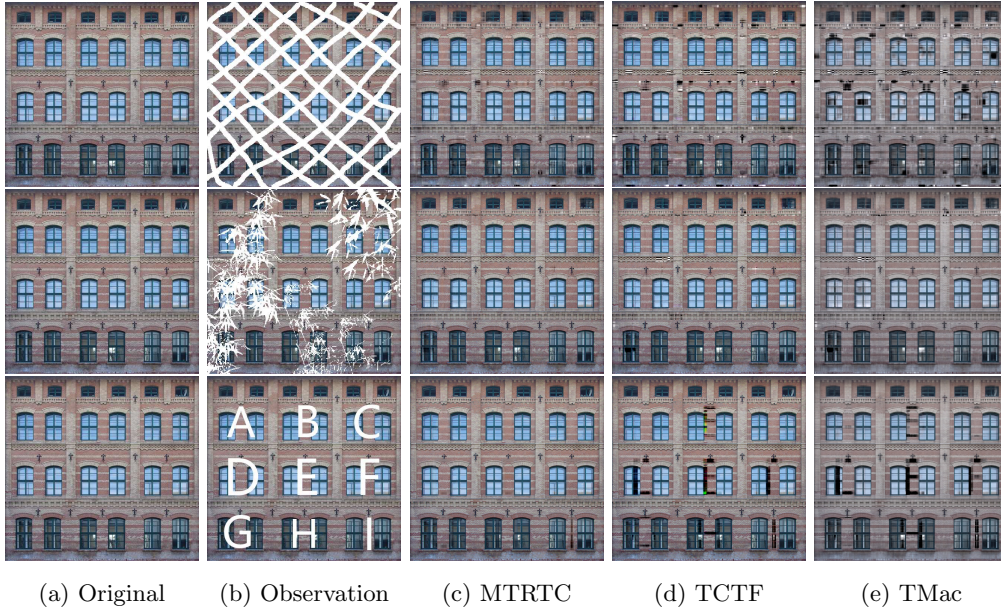


Figure 6: Recovery performance comparison on the three masked images

Table 2: Comparison on the PSNR and the RSE by MTRTC, TCTF and TMac

Mask \ Method	MTRTC		TCTF		TMac	
	PSNR	RSE	PSNR	RSE	PSNR	RSE
Grid	25.26	0.1048	22.57	0.1429	20.31	0.1854
Leaves	30.16	0.0596	28.69	0.0706	25.91	0.0972
Letters	30.82	0.0553	23.00	0.1359	21.70	0.1579

5.3 Video Simulation

We evaluate our proposed methods MTRTC and ST-MTRTC on the widely used YUV Video Sequences². Each sequence contains at least 150 frames and we pick the first 60 frames. In the experiments, we test our proposed methods and other methods on three videos with 144×176 pixels. We test the videos with random missing data of sampling ratio $p = 0.3$. We set the initial multi-tubal rank $(r_u^l)^0 = 10, u \in [2], (r_3^l)^0 = 60, l \in [\mathbf{n}_u]$ in MTRTC and ST-MTRTC, the initial tubal rank $(30, 30, 30)$ in TCTF and the initial Tucker rank $(60, 60, 10)$ in TMac. In experiments, the maximum iteration number is set to be 800 and the termination precision ε is set to be $1e-5$.

The data between two adjacent frames of the video usually have not drastic change. To detect such stability, we calculate the data pairs of the corresponding positions between two adjacent frames. The difference for two adjacent frames of the video slots (k and $k + 1$) is defined as

$$frame(i, j, k) = |C_3^k(i, j) - C_3^{k+1}(i, j)|.$$

The smaller the $frame(i, j, k)$ is, the more stable the data between two adjacent frames of the video at frame k is. By computing the normalized difference values between two adjacent frames, we measure the stability between two adjacent frames of the video at frame k as

$$\Delta gap(i, j, k) = \frac{|C_3^k(i, j) - C_3^{k+1}(i, j)|}{\max_{1 \leq i \leq n_1, 1 \leq j \leq n_2, 1 \leq k \leq n_3 - 1} |C_3^k(i, j) - C_3^{k+1}(i, j)|}.$$

Here $\max_{1 \leq i \leq n_1, 1 \leq j \leq n_2, 1 \leq k \leq n_3 - 1} |C_3^k(i, j) - C_3^{k+1}(i, j)|$ means the maximal gap between any two adjacent frames of the video. We plot the CDF of $\Delta frame(i, j, k)$ in Figure 7. The X-axis represents the normalized difference values between two adjacent frames slots, i.e., $\Delta frame(i, j, k)$. The Y-axis represents the cumulative probability. We can see that the value $\Delta frame(i, j, k) < 0.6$ is more than 80%. These results indicate that the temporal stability exists in the real video data. Hence we apply ST-MTRTC in video inpainting with Toeplitz matrix being a temporal constrained matrix H . Furthermore, $\beta_1 = \beta_2 = 0$, which mean that F and G are zero matrices.

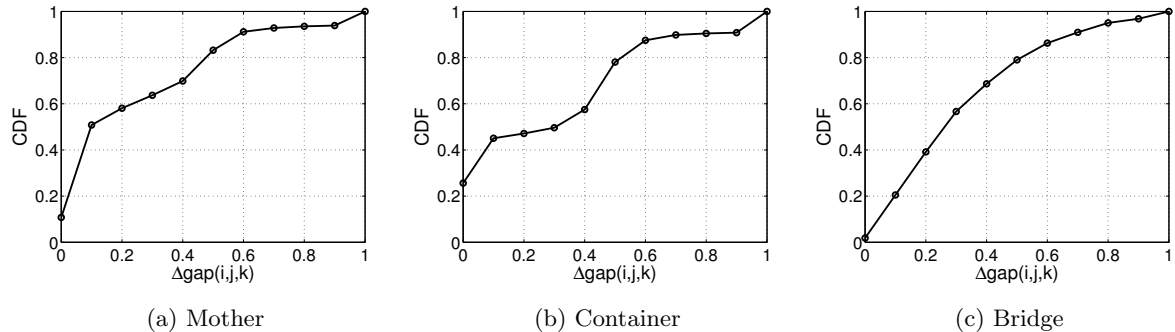


Figure 7: An empirical study of three sets of real video data

Figure 8 shows the 18th frame of the three videos. Table 3 displays the numerical results, which show that MTRTC performs better than TCTF and TMac on PSNR and RSE. Especially for the container

²<http://trace.eas.asu.edu/yuv/>

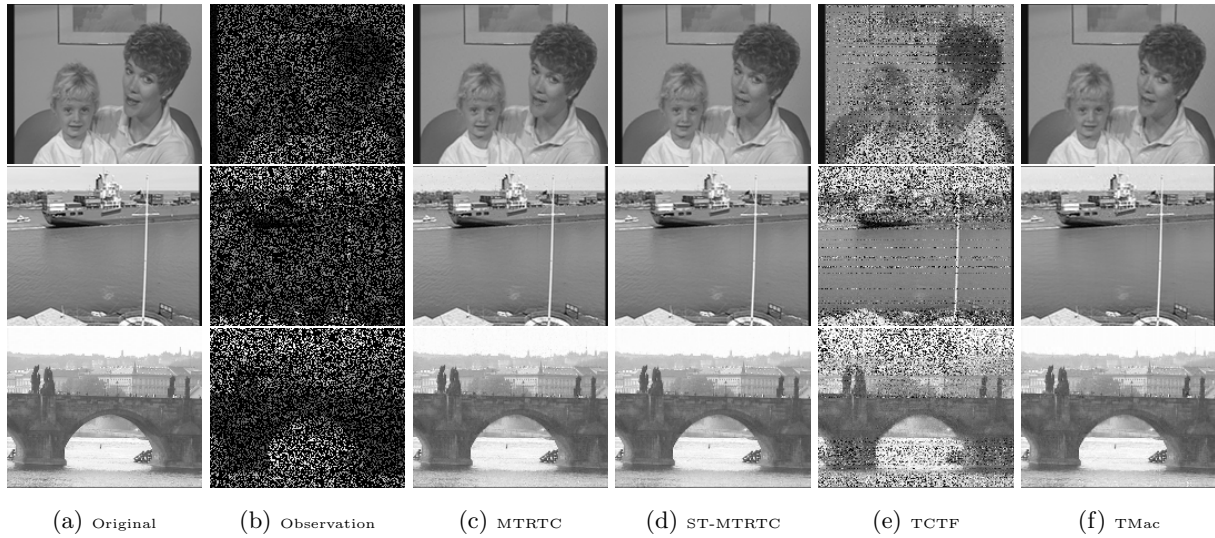


Figure 8: Recovery performance comparison on the three videos

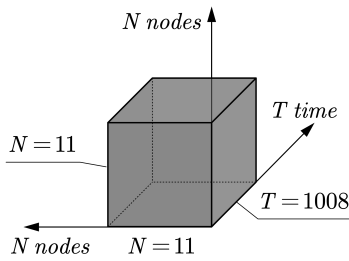
Table 3: Comparison on the PSNR, the RSE and the running time on the three videos

Method \ Video	Mother			Container			Bridge		
	PSNR	RSE	time	PSNR	RSE	time	PSNR	RSE	time
MTRTC	37.02	0.024	34.14	40.53	0.016	50.46	34.79	0.026	36.74
ST-MTRTC	37.79	0.022	46.33	42.58	0.012	60.63	35.55	0.024	33.37
TCTF	14.19	0.338	94.59	13.11	0.367	95.82	11.93	0.357	93.45
TMac	35.92	0.028	39.11	34.45	0.032	77.77	33.88	0.028	38.84

video, PSNR of MTRTC has increased by 209.53% and 26.36% over TCTF and TMac, respectively. On consumed time, MTRTC also takes the least time to recover the three videos among all algorithms.

Numerical results displayed in Table 3 show that ST-MTRTC performs better than MTRTC on PSNR and RSE. The consumed time of ST-MTRTC is similar to MTRTC. Even in container video, the PSNR returned by ST-MTRTC has increased by 5.06% over MTRTC. These results indicate that the temporal stability exists in the real video data, which improves the performance of MTRTC.

5.4 Internet Traffic Simulation



We model the traffic data as a third order tensor $\mathcal{M} \in \mathbb{R}^{D \times T \times O}$. Here O corresponds to the number of OD pairs with $O = N \times N$ (N is the number of nodes in the network), and there are D days to consider with each day having T time slots.

We use Abilene trace data [35] as an example to illustrate this model. The traffic data are collected between 144 OD pairs in 168 days, and the measurements are made every 5 minutes which corresponds to 288 time slots every day. We use a complete one week traffic data. Therefore, the trace data can be modeled as a third order tensor $\mathcal{M} \in \mathbb{R}^{7 \times 288 \times 144}$. We use the normalized mean absolute error (NMAE) in the missing values as a metric of the recovered data. The NMAE is defined as follows

$$\text{NMAE} = \frac{\sum_{(i,j,k) \notin \Omega} |\mathcal{M}_{ijk} - \hat{\mathcal{C}}_{ijk}|}{\sum_{(i,j,k) \notin \Omega} |\mathcal{M}_{ijk}|}$$

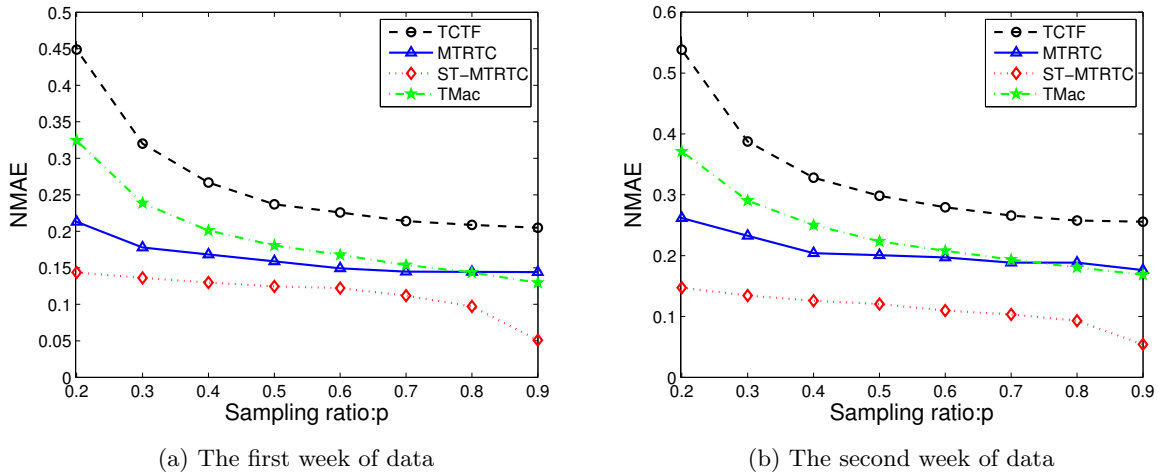


Figure 9: Comparison on the NMAE by four methods of different sampling ratios

Figure 9 shows the recovered results in Abilene dataset by four algorithms. The X-axis represents the sample rate of data, and the Y-axis represents RSE. As the sample rate increases, the RSE value

gradually decreases. Among the four methods, ST-MTRTC has the best recovery effect. Note that ST-MTRTC can still recover lost data with very low error even if the sample rate is very low. Furthermore, MTRTC lags behind ST-MTRTC, which means a spatio-temporal structure in the network traffic data works well.

For further comparison, we illustrate the recovered data for the 139th OD pair of Abilene data. To this end, we select the first 144 data per day. As shown in Figure 10, some of data recovered by TCTF and TMac are far from the original data when the sample rate is lower than $p = 0.6$. However, the data recovered by ST-MTRTC fits the original data well. That is, ST-MTRTC can recover the data of low sample rate with high accuracy. Although the accuracy of the TCTF and TMac methods raise with the increasing of sample rate, ST-MTRTC also outperforms TCTF and TMac. These results indicate that ST-MTRTC is the best method to recover internet traffic data.

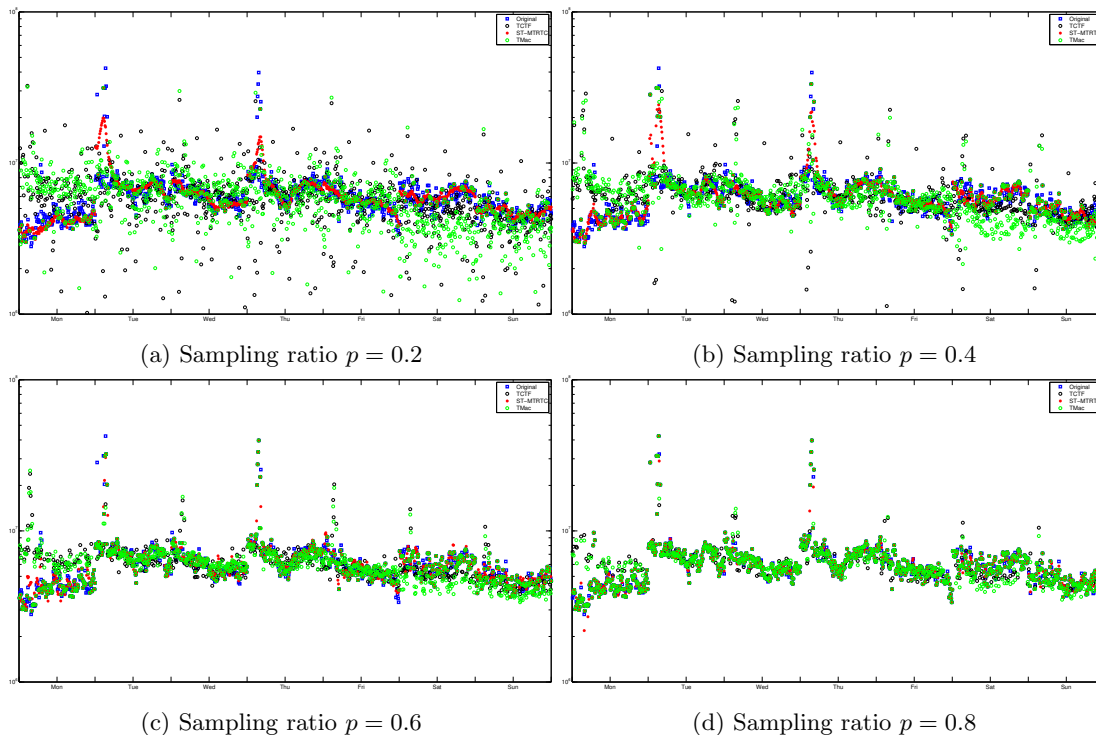


Figure 10: Recovery performance comparison of different sampling ratios

6 Conclusion

In this paper, we extended tubal rank to multi-tubal rank and then established a relationship between multi-tubal rank and Tucker rank. The tubal rank focuses on one mode of the tensor, while multi-tubal rank considers all three modes of the tensor together. Based on multi-tubal rank, we established a new tensor completion model and applied a tensor factorization based method for solving the established problem. In addition, we applied spatio-temporal characteristics to the video inpainting and internet traffic simulation to modify the established model as a novel one. A modified tensor factorization based method was presented to solve such data completion problem, which got better performance without

increasing the computational cost. Experimental results showed that the performance of our proposed methods were significantly better than existing methods in the literature.

References

- [1] D. Alderson, H. Chang, M. Roughan, S. Uhlig and W. Willinger, “The many facets of internet topology and traffic”, *Networks and Heterogeneous Media*, 1 (2006), 569-600.
- [2] M. Asif, N. Mitrovic, J. Dauwels and P. Jaillet, “Matrix and tensor based methods for missing data estimation in large traffic network”, *IEEE Transactions on Intelligent Transportation Systems*, 17 (2016), 1816-1825.
- [3] H. Attouch, J. Bolte and B. Svaiter, “Convergence of descent methods for semi-algebraic and tame problems: proximal algorithms, forward-backward splitting, and regularized Gauss-Seidel methods”, *Mathematical Programming*, 137 (2013), 91-129.
- [4] M. Bai, X. Zhang, G. Ni and C. Cui, “An adaptive correction approach for tensor completion”, *SIAM Journal on Imaging Sciences*, 9 (2016), 1298-1323.
- [5] J. Bengua, H. Phien, H. Tuan and M. Do, “Efficient tensor completion for color image and video recovery: low-rank tensor train”, *IEEE Transactions on Image Processing*, 26 (2017), 2466-2479.
- [6] J. Carroll and J. Chang, “Analysis of individual differences in multidimensional scaling via an N-way generalization of “Eckart-Young” decomposition”, *Psychometrika*, 35 (1970), 283-319.
- [7] J. Chang, Y. Chen, L. Qi and H. Yan, “Hypergraph clustering using a new Laplacian tensor with applications in image processing”, *SIAM Journal on Imaging Sciences*, 13 (2020), 1157-1178.
- [8] S. Gandy, B. Recht and I. Yamada, “Tensor completion and low-n-rank tensor recovery via convex optimization”, *Inverse Problems*, 27 (2011), 025010.
- [9] N. Hao, M. Kilmer, K. Braman and R. Hoover, “Facial recognition using tensor-tensor decompositions”, *SIAM Journal on Imaging Sciences*, 6 (2013), 437-463.
- [10] C. Hillar and L. Lim, “Most tensor problems are NP-hard”, *Journal of the ACM*, 60 (2013) 39.
- [11] W. Hu, D. Tao, W. Zhang, Y. Xie and Y. Yang, “The twist tensor nuclear norm for video completion”, *IEEE Transactions on Neural Networks and Learning Systems*, 28 (2017), 2961-2973.
- [12] F. Jiang, X. Liu, H. Lu and R. Shen, “Anisotropic total variation regularized low-rank tensor completion based on tensor nuclear norm for color image inpainting”, *IEEE International Conference on Acoustics, Speech and Signal Processing (ICASSP)*, (2018), 1363-1367.
- [13] H. Kasai, “Online low-rank tensor subspace tracking from incomplete data by CP decomposition using recursive least squares”, *IEEE International Conference on Acoustics, Speech and Signal Processing (ICASSP)*, (2016), 2519-2523.
- [14] H. Kiers, “Towards a standardized notation and terminology in multiway analysis”, *Journal of Chemometrics*, 14 (2000), 105-122.

- [15] M. Kilmer, K. Braman, N. Hao and R. Hoover, “Third-order tensors as operators on matrices: a theoretical and computational framework with applications in imaging”, *SIAM Journal on Matrix Analysis and Applications*, 34 (2013), 148-172.
- [16] M. Kilmer and C. Martin, “Factorization strategies for third-order tensor”, *Linear Algebra and its Applications*, 435 (2011), 641-658.
- [17] T. G. Kolda and B. W. Bader, “Tensor decompositions and applications”, *SIAM Review*, 51 (2009), 455-500.
- [18] P. M. Kroonenberg, “Three-mode principal component analysis: theory and applications”, Leiden: DSWO Press, 1983.
- [19] L. Lathauwer and B. Moor, “From matrix to tensor: multilinear algebra and signal processing”, *Mathematics in Signal Processing IV*, (1997), 1-15.
- [20] L. Lathauwer and J. Vandewalle, “Dimensionality reduction in higher-order signal processing and rank- (R_1, R_2, \dots, R_N) reduction in multilinear algebra”, *Linear Algebra and its Applications*, 391 (2004), 31-55.
- [21] S. Li and Q. Liu, “Multi-filters guided low-rank tensor coding for image inpainting”, 2nd International Conference on Image, Vision and Computing (ICIVC), (2017), 418-422.
- [22] J. Liu, P. Musialski, P. Wonka and J. Ye, “Tensor completion for estimating missing values in visual data”, *IEEE Transactions on Pattern Analysis and Machine Intelligence*, 35 (2013), 208-220.
- [23] Y. Liu, Z. Long and C. Zhu, “Image completion using low tensor tree rank and total variation minimization”, *IEEE Transactions on Multimedia*, 21 (2019), 338-350.
- [24] Y. Liu and F. Shang, “An efficient matrix factorization method for tensor completion”, *IEEE Signal Processing Letters*, 20 (2013), 307-310.
- [25] Z. Long, Y. Liu, L. Chen and C. Zhu, “Low rank tensor completion for multiway visual data”, *Signal Processing*, 155 (2019), 301-316.
- [26] C. Lu, J. Feng, Y. Chen, W. Liu, Z. Lin and S. Yan, “Tensor robust principal component analysis: exact recovery of corrupted low-rank tensors via convex optimization”, *The IEEE Conference on Computer Vision and Pattern Recognition (CVPR)*, (2016), 5249-5257.
- [27] D. Martin, C. Fowlkes, D. Tal and J. Malik, “A database of human segmented natural images and its application to evaluating segmentation algorithms and measuring ecological statistics”, *Proceedings Eighth IEEE International Conference on Computer Vision. ICCV 2001*, 2 (2001), 416-423.
- [28] C. Martin, R. Shafer and B. LaRue, “An order-p tensor factorization with applications in imaging”, *SIAM Journal on Scientific Computing*, 35 (2013), 474-490.
- [29] B. Mitchell and D. Burdick, “Slowly converging PARAFAC sequences: swamps and two-factor degeneracies”, *Journal of Chemometrics*, 8 (1994), 155-168.
- [30] D. Muti and S. Bourennane, “Multidimensional filtering based on a tensor approach”, *Signal Processing*, 85 (2005), 2338-2353.

- [31] M. Roughan, Y. Zhang, W. Willinger and L. Qiu, “Spatio-temporal compressive sensing and internet traffic matrices”, *IEEE/ACM Transactions on Networking*, 20 (2012), 662-676.
- [32] A. Smilde, R. Bro and P. Geladi, “Multi-way analysis: applications in the chemical sciences”, *Technometrics*, 47 (2004), 518-519.
- [33] H. Tan, Y. Wu, B. Shen, P. J. Jin and B. Ran, “Short-term traffic prediction based on dynamic tensor completion”, *IEEE Transactions on Intelligent Transportation Systems*, 17 (2016), 2123-2133.
- [34] L. Tucker, “Some mathematical notes on three-mode factor analysis”, *Psychometrika*, 31 (1966), 279-311.
- [35] The Abilene Observatory Data Collections. Accessed: 2013. [Online]. Available: <http://abilene.internet2.edu/observatory/data-collections.html>.
- [36] M. Vasilescu and D. Terzopoulos, “Multilinear analysis of image ensembles: tensorfaces”, *European Conference on Computer Vision*, (2002), 447-460.
- [37] Z. Wen, W. Yin and Y. Zhang, “Solving a low-rank factorization model for matrix completion by a nonlinear successive over-relaxation algorithm”, *Mathematical Programming Computation*, 4 (2012), 333-361.
- [38] Y. Xu, R. Hao, W. Yin and Z. Su, “Parallel matrix factorization for low-rank tensor completion”, *Inverse Problems and Imaging*, 9 (2013), 208-220.
- [39] X. Zhang and M. Ng, “A corrected tensor nuclear norm minimization method for noisy low-rank tensor completion”, *SIAM Journal on Imaging Sciences*, 12 (2019), 1231-1273.
- [40] Z. Zhang, G. Ely, S. Aeron, N. Hao and M. Kilmer, “Novel methods for multilinear data completion and de-noising based on tensor-SVD”, *IEEE Conference on Computer Vision and Pattern Recognition*, (2014), 3842-3849.
- [41] H. Zhou, D. Zhang, K. Xie and Y. X. Chen, “Spatio-temporal tensor completion for imputing missing internet traffic data”, *International Performance Computing and Communications Conference*, (2015), 1-7.
- [42] P. Zhou, C. Lu, Z. Lin and C. Zhang, “Tensor factorization for low-rank tensor completion”, *IEEE Transactions on Image Processing*, 27 (2018), 1152-1163.